# Heralded arbitrary graph states with inefficient quantum emitters

Maxwell Gold,<sup>1,\*</sup> Jianlong Lin,<sup>2,\*</sup> Eric Chitambar,<sup>2</sup> and Elizabeth A. Goldschmidt<sup>1</sup>

<sup>1</sup>Department of Physics, University of Illinois Urbana-Champaign, Urbana, IL 61801

<sup>2</sup>Department of Electrical and Computer Engineering,

University of Illinois Urbana-Champaign, Urbana, IL 61801

(Dated: May 24, 2024)

Quantum emitter-based schemes for the generation of photonic graph states offer a promising, resource efficient methodology for realizing distributed quantum computation and communication protocols on near-term hardware. We present a heralded scheme for making photonic graph states that is compatible with the typically poor photon collection from state-of-the-art coherent quantum emitters. We demonstrate that the construction time for large graph states can be polynomial in the photon collection efficiency, as compared to the exponential scaling of current emitter-based schemes, which assume deterministic photon collection. The additional overhead to achieve this advantage consists of an extra spin system plus one additional spin-spin entangling gate per photon added to the graph. While the proposed scheme enables the generation of graph states for arbitrary applications, we show how it can be further simplified for the specific task of measurement-based computation, leading to significantly higher rates and removing the need for photonic memory in certain computations. As an example use-case of our scheme, we construct a protocol for secure two-party computation that can be implemented efficiently on current hardware. Estimates of the fidelity to produce graph states used in the computation are given, based on current trapped ion experimental benchmarks.

#### I. INTRODUCTION

The vast promise of quantum information technologies for faster and more secure computational and information systems relies on entanglement as a primary resource. Traditional gate-based quantum computing requires the ability to perform sequences of joint operations across multiple qubits. An alternative paradigm, known as measurement-based quantum computation (MBQC), realizes universal computation through sequences of single qubit measurements made on an initially prepared entangled resource state [1]. This is an appealing approach for photonic quantum systems as single photon rotations and measurements are straightforward using commercial optical elements, and fast efficient routing solutions are readily available [2]. Furthermore, the sequential nature of photon emission allows entangled states to be built from photons emitted at different times by the same emitter [3]. By using entangled emitters, it then becomes possible to simulate entangling gates between photons and overcome the difficulty of realizing direct photon-photon interactions [4]. Indeed, it is known that computationally useful graph states of photons can be generated using either a small number of coherent quantum emitters [5], a combination of a single emitter and fusion gates [6], or a single quantum emitter in a feedback scheme [7].

All of these aforementioned schemes assume a photon is successfully added to the graph every time an emitter is excited, and we thus term this class of schemes as being "deterministic". However, efficient collection from individual quantum emitters is a challenge that remains largely out of reach today, making deterministic

schemes impractical for generating large graph states on even near-term hardware [8].

We introduce a procedure for building arbitrary photonic graph states using a single emitting spin and a fixed number of auxiliary spins, without any requirement on the collection efficiency of the emitted photons. The rate and size of feasible graph states generated by the proposed method has polynomial dependence on the collection efficiency, compared to the exponential suppression of the feasible graph size for the successive detection of photons required in current deterministic schemes. This enhanced performance is achieved by recognizing the possibility of adding each photon to the graph only after successful spin-photon entanglement generation has been heralded.

In Section II of this work, we describe a non-destructive method for this heralding that is implementable on current hardware by swapping the entanglement to another photon, termed the herald-on-swap (HoS) method. More generally, any non-destructive detection of the photon would be suitable to implement this "emit then add" method of building graphs for arbitrary use. We explain in Section III how we can herald on destructive detection of the photon in certain cases, including MBQC. This enables much higher production rates and fidelities than any feasible non-destructive heralding method. In this case, the emitted photon is measured prior to adding it to the graph, thereby abrogating the need for entanglement swapping or photon storage, and dramatically speeding up graph construction. In this case, the graph state is built only virtually as every photon in the graph is necessarily measured. We refer to this as a herald-ondetection (HoD) method, and Section III provides more detail on when the HoD method can be applied.

In both the HoS and HoD schemes we propose, the

<sup>\*</sup> These two authors contributed equally

photons are emitted over a longer time, when compared to other emitter-based methods for building photonic graph states; this is because most attempts to add a photon to the graph will result in an unsuccessful herald. Consequently, it is the number of excitation attempts that can be made during the coherence time of the emitter that sets the practical limit on the graph size, rather than the collection efficiency. Trapped neutral atoms and ions in vacuum are well suited to this scheme as they exhibit long coherence times  $(10^0 - 10^3 \text{ seconds})$  [9, 10] and host high-fidelity deterministic entangling gates (> 99%) [11–13] with moderate collection efficiencies ( $\gtrsim 10\%$  with high-NA optics and  $\gtrsim 40\%$  with parabolic reflectors) [14– 17]. We note here that some solid-state systems, such as rare-earth emitters, can also exhibit excellent coherence, spin-spin entangling gates, and reasonable photon collection via integration into photonic devices [18]. In Section IV we provide estimates of the rate and fidelity for the production of heralded graph states via both of our schemes assuming state-of-the-art trapped ion and photon pair source architectures, which include realistic sources of loss, noise, and decoherence.

Lastly, in Section V we propose a protocol for performing secure two-party classical computation, in which two parties privately compute a function of their input variables with the help of an untrusted referee. Compared to universal quantum computation, our protocol only requires Pauli measurements, and so the entire procedure can be performed using only our HoD method. We demonstrate how secure two-party computation can be achieved using just a single quantum emitter and two auxiliary spin gubits, regardless of the size of the party's input. We provide fidelity estimates to produce the graph states on current hardware, which suggests this is a highly feasible use-case for quantum networks in the near term. A security analysis and the resulting bit error rates with and without classical error correction are also provided.

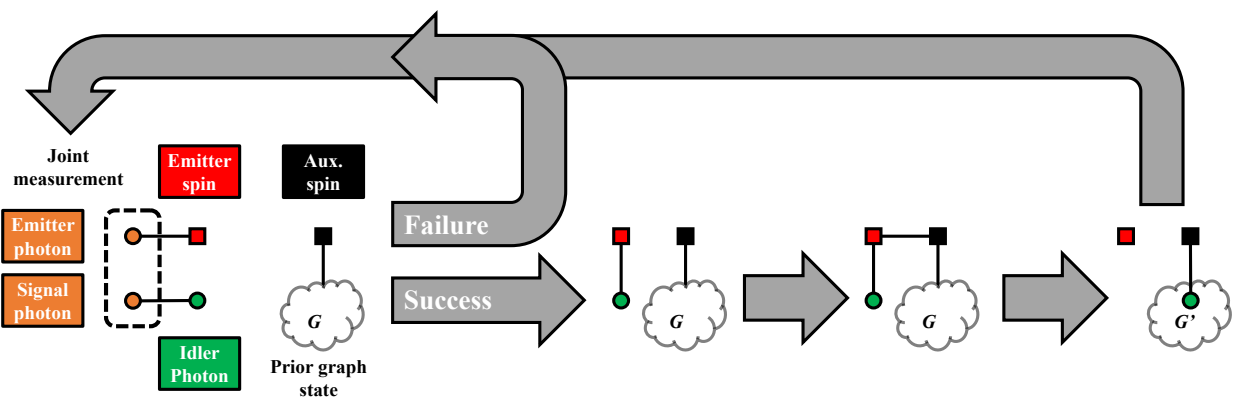
# II. SPIN-PHOTON ENTANGLEMENT SCHEMES

We first describe the HoS scheme, shown in Figure 1, for making graph states for arbitrary applications. Given the technical challenges associated with photon non-demolition measurement [19], this swapping step is required to herald without destructive measurement of the photonic qubit on near-term hardware. Compared to the deterministic scheme described in [5], we include a local entanglement swapping step between an emitter-photon entangled pair and a pair of entangled photons, and only add the final photon to the graph upon success of that swap. A single emitter is initialized onto an unentangled state and excited to produce a single photon that is entangled with its long-lived internal spin state and collected with some overall efficiency  $\eta_e$ . This can be implemented with a wide variety of quantum emitters includ-

ing laser-cooled atoms or ions, quantum dots, and defects or dopants in wide-bandgap semiconductors [3, 8, 20–22]. Photons can be encoded in various degrees of freedom including polarization, time-bin, and frequency [23–27]. Simultaneously, a pair of entangled photons is probabilistically produced, which can be implemented via standard nonlinear optical processes, such as spontaneous parametric down conversion (SPDC) [28, 29]. One member of the photon pair, the signal photon, is wavelength and bandwidth matched to the emitter photon, and the entangled pair is encoded in the same degree of freedom as the emitter photon. The emitter photon and signal photon are sent to a joint measurement apparatus which, upon a successful measurement outcome, projects the emitter spin and the unmeasured photon, the idler photon, onto an entangled Bell state [30]. Since only certain measurement outcomes correspond to entanglement between the emitter spin and idler photon, and imperfect collection and detection means that fewer than two photons are detected on most attempts, the procedure is repeated until a successful herald is flagged. Following each failed attempt, the emitter is measured and reinitialized for the subsequent attempt at a successful herald.

We assume the emitter is among a set of spin qubits that can be controllably entangled in a pair-wise way via local and deterministic two-qubit spin-spin entangling gates, such as an array of trapped atomic ions or neutral atoms. Upon a successful herald, the emitter spin is deterministically entangled with an auxiliary spin, which may already be part of a larger graph state. The emitter spin is then rotated to a conjugate basis and projectively measured, removing it from the graph without disturbing any of the other qubits. Following a correction to the photon based on the outcome of this measurement, the state of the system is as if the auxiliary spin had directly emitted the photon itself. This "emit then add" method then allows for the construction of arbitrary photonic graph states using the methods described in [5]. Namely, the graph states are built using sequences of two-qubit gates on the spins and local Clifford gates on the photons. The local gates on each photon can all be combined and applied as a single rotation prior to using the graph state in subsequent applications.

The key improvement in our scheme is that the idler photon can be collected with near unit efficiency upon a successful herald [31]. Attaining the improvement of this scheme requires one additional two-qubit spin-spin entangling gate per photon added to the graph plus one additional spin (the emitter), compared to the requirements for generating graphs via known deterministic schemes [32]. In addition, the graph is emitted over a much longer time and thus requires longer spin coherence times. We note an additional benefit of the scheme in that the idler photon can be at virtually any wavelength due to the flexibility of standard entangled photon pair sources [33–36], which overcomes common challenges due to the inconvenient emission colors of many atomic qubits. We show here that current state-of-the-art trapped ion sys-



Attempt herald

Pass heralded idler photon to graph

FIG. 1. Herald-on-swap (HoS) scheme. The components are two initial entangled pairs: an emitter spin (red square) entangled with a photon (orange circle) and a signal-idler entangled photon pair (orange and green circle, respectively). We also assume an existing graph G that contains one or more auxiliary spins (black square). Entanglement swapping is attempted between the two initial entangled pairs. Upon success, a two-qubit spin-spin gate deterministically entangles the emitter spin and auxiliary spin. A local complementation operation is then performed on the emitter spin, which is subsequently measured out of the graph. This leaves the idler photon a part of the graph and the emitter spin reinitialized for the next attempted emission.

tems can be designed to produce graph states of tens to hundreds of photons using the proposed method, where extending to thousands would be made possible with reasonable improvements [10, 12, 14].

# III. A HERALDING SCHEME FOR MBQC

The HoS scheme described in the previous section, or any non-destructive heralding of successful collection of the emitter photon, can be used to build arbitrary photonic graph states. However, for many applications, including MBQC, the nodes are measured sequentially with the choice of measurement basis on one node depending on outcomes of previous ones. It is not necessary in this case to build the full graph state before beginning these measurements [37]. Instead, an emitted photon can be destructively measured as soon as the correct basis for measurement is determined. This measurement thus serves doubly as a prescribed step in the MBQC protocol and as a way for detecting the emitted photon. Upon failure to detect the photon, we reinitialize the emitter and attempt generation again, having left the larger graph undisturbed, as in the HoS scheme. Upon successful detection, we perform all required gates on the emitter and auxiliary spins, measure the emitter out of the graph, and reinitialize the emitter to attempt generation of the next photon in the graph.

This simpler HoD scheme is shown in Figure 2, and it has the advantage that it requires no storage time for the emitted photon prior to measurement. There are limitations for when this scheme can be employed. Namely, a photon can be measured using HoD provided the two con-

ditions are satisfied: (1) the correct measurement basis for that photon, as set by the MBQC protocol, is determined prior to its emission, and (2) this measurement is either Pauli Z or of the form  $\cos\phi X + \sin\phi Y$ . Condition (1) can be met in general, as the emission order can be chosen to match the measurement order of the computation, albeit at the cost of using extra auxiliary spins and two-qubit gates in some cases [32]. The second condition can also be met in principle, since the specified gate sets are sufficient for universal MBQC [1, 38].

To understand condition (2) in more detail, note that if the full graph state were built using HoS and two-qubit gates on the auxiliary spins, then each emitted photon would have a local Clifford error of the form  $UZ^m$ , where U is a fixed Clifford and  $m \in \{0,1\}$  is determined by the decoupling measurement on the emitter spin. If M is the measurement to be subsequently performed on the photon in the MBQC protocol, then when correcting for the Clifford error, the effective measurement would be  $M' = UZ^m MZ^m U^{\dagger}$ . When M = Z, then  $M' = UZU^{\dagger}$ ; or when  $M = \cos \phi X + \sin \phi Y$ , then  $M' = (-1)^m U Z U^{\dagger}$ . In the first case, the dependence on m is completely removed, and the photon can be equivalently measured with  $UZU^{\dagger}$  immediately after it is emitted in the HoD scheme. In the second case, it can also be immediately measured with  $UZU^{\dagger}$ , but now one must perform a bit flip on the classical measurement outcome if m = 1; this is because an overall -1 factor on a spin observable simply flips the spin-up/spin-down outcomes. In summary, the correct computation can be attained through HoD and classical post-processing for observables of the specified form.

While satisfying conditions (1) and (2) above is suffi-

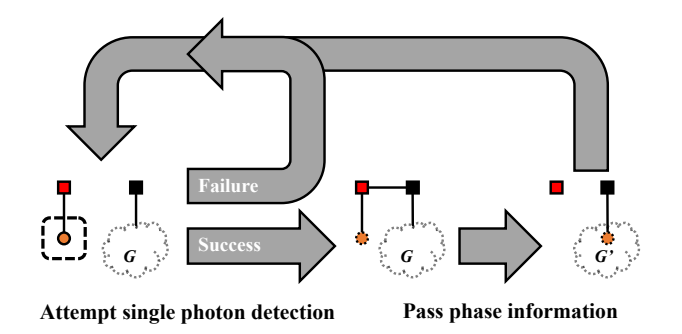


FIG. 2. Herald-on-detection (HoD) scheme. For certain MBQC protocols, it is sufficient to perform the deterministic entangling gate between the emitter and auxiliary spin only upon successful detection of the emitted photon. The photonic graph state constructed in this case is virtual (represented by dashed boundaries) and exists as a set of conditional phases stored on the auxiliary spin(s).

cient for universal MBQC using HoD, this is often not the most efficient method in terms of the overall number of photons used to drive the computation. For example, building out the graph to a certain depth and measuring in a different sequence than the emission order can lead to more compact gate implementations [38]. Also, using MBQC measurements outside of the x-y plane allows for more general forms of information flow [39]. Nevertheless, as we show in the next section, the HoD scheme can enable dramatically faster construction and higher fidelity with no photon storage required. For the HoS (or any non-destructive heralding) scheme, photon storage is required for at least the time to perform the spin-spin entangling gates and the decoupling measurement on the emitter.

# IV. SCALING AND FIDELITY FOR HERALDED SCHEMES

A major benefit of both schemes comes in scaling up the size of graph states using near term hardware. The average time to successfully generate an  $n_p$ -photon graph by directly collecting photons from an emitter in  $n_p$  subsequent excitation events for computation is  $\mathcal{O}(\eta_e^{-n_p})$ , where  $\eta_e$  is the emitter collection efficiency, as any failed detection event truncates the graph. In typical deterministic quantum emitter-based schemes, any inefficiency in collection therefore leads to exponentially bad scaling with graph size. Given current hardware, this severely limits the size and rate of generation for photonic graph states, particularly those that require multiple spin qubits. We note that there are loss tolerance and percolation thresholds that improve this scaling, but they require much better collection efficiency than is feasible in near-term systems [40–42]. For the heralded schemes, any failed detection of the emitter photon simply results in the reinitialization of the emitter and another attempt

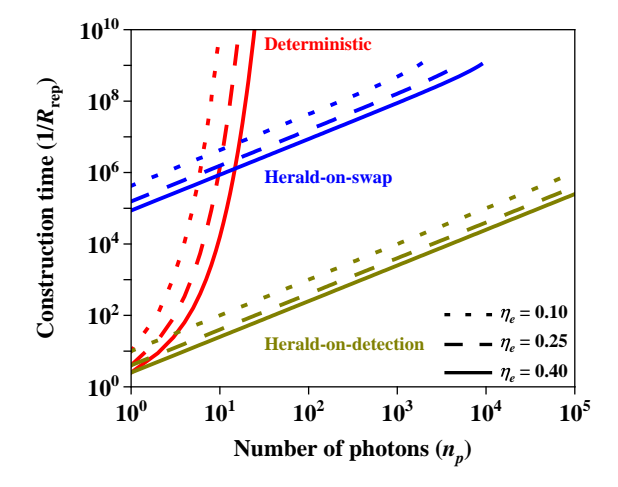


FIG. 3. Time to make photonic graph states of size  $n_p$  in units of the repetition period. The deterministic (red), HoS (blue), and HoD (yellow) schemes are compared. The three curves of each color represent emitter photon collection efficiencies  $\eta_e \in \{0.1, 0.25, 0.4\}$ . Polynomial scaling in the heralded schemes allows for the construction of larger graphs. Results are omitted where decoherence and false heralds bring the fidelity under 50% for reasonable experimental parameters. In the HoS scheme, fidelity can be sacrificed to improve the rate for the construction of small graph states if desired. A full description of these estimates is given in Appendix D.

at the joint or single photon detection, while the graph under construction remains unaffected. Therefore, an  $n_p$ photon graph state will be created over a time that is  $\mathcal{O}(n_p\eta_e^{-1})$ . As a comparison, the time to make an  $n_p$ photon graph state (in units of the repetition period) is shown in Figure 3 for  $\eta_e \in \{0.1, 0.25, 0.4\}$  for the deterministic (red), HoS (blue), and HoD (yellow) schemes. We do not include the time to perform gates and measurements on the spins for these estimates, and we assume that the emitter coherence does not limit the graph size for the deterministic scheme  $(n_p/\tau R_{\rm rep}\ll 1$  where  $\tau$ is the spin coherence time and  $R_{\rm rep}$  is the repetition rate of excitation). In practice, however, the short coherence times of the most efficient photon emitters further limit the size of graphs that can be produced in the deterministic scheme [8, 27]. For the heralded schemes, all auxiliary spins must remain coherent for the entire time they are a part of the graph, which is much longer than the  $n_p$  repetition cycles over which the graph is generated in the deterministic scheme. Thus, moving from the deterministic scheme to one proposed here effectively means moving from a scheme limited by the photon collection efficiency to a scheme limited by spin coherence. If a hybrid of the HoS and HoD schemes is employed, the generation time falls somewhere between the curves for those schemes, with the fraction of photons generated via each method determining exactly where.

For the two proposed schemes, there are additional factors that affect the fidelity that are not present in the de-

terministic scheme, including decoherence of the emitter and auxiliary spin(s) during the construction time and multiple photon pair production that limits the fidelity of entanglement swapping for the HoS scheme. Here we investigate the scaling of these sources of infidelity and compare them to the limits set by imperfect two-qubit spin-spin entangling gates, as well as the initial entanglement fidelities of the emitter photon and photon pair sources. We require one extra spin-spin entangling gate each time we add a photon to the graph, in addition to the gates required to make the desired final graph [32], which exponentially suppresses the fidelity of large photonic graph states if the gates are not perfect. Additionally, any infidelity of the photon pair source in the HoS scheme adds to the overall infidelity. Here, we demonstrate that if sufficient error correction or entanglement purification is possible [43], the additional sources of infidelity inherent to our scheme do not themselves prohibit exceedingly large graph states. For a full discussion of our experimental model and relevant sources of infidelity, see Appendix D.

In modeling decoherence under the usual dephasing map, any emitters or auxiliary spins will remain invariant with a probability  $D(t,\tau) = \frac{1}{2}(1+e^{-t/\tau})$ , for the duration t until they are projectively measured. In either scheme, the emitter is reinitialized with each attempt to add a new photon to the larger graph, and hence the time it is required to remain coherent is reset. Furthermore, the classical conditioning offered by this "emit then add" method means the emitter is only required to remain coherent for the attempts where the relevant joint or single photon measurements are a success. Any auxiliary spins, on the other hand, are required to remain coherent for the duration of time they remain a part of the larger graph state in construction. The average time for the successful addition of a new photon to the larger graph goes as  $t_{\rm rep}/P_s$ , where  $t_{\rm rep}=R_{\rm rep}^{-1}$  is the repetition period of the excitation, and  $P_s$  is the probability of a successful joint or single photon measurement for the HoS or HoD schemes, respectively. Note that in the HoD scheme we assume  $P_s = \eta_e$ . Hence, the total contribution to the final state fidelity from the emitter and any auxiliary spins

$$F_D^{(e)}(n_p) = \left(\frac{1}{2}\left(1 + e^{-t_{\rm rep}/\tau}\right)\right)^{n_p},$$
 (1a)

$$\langle F_D^{(s)}(n_p, P_s) \rangle = \frac{1}{2} \left( 1 + e^{-n_p t_{\text{rep}}/P_s \tau} \right), \qquad (1b)$$

where we include a superscript to denote emitter (e) and auxiliary spin (s) qubits, and we have used the same coherence time  $\tau$  for the emitter and auxiliary spins in the system.

For the HoS scheme, we assume a standard SPDC source to generate the required entangled photon pairs [44]. The multi-pair emission of such a source introduces an additional infidelity in the entanglement swapping procedure. We denote  $P_t$  as the overall probability that a true Bell state is heralded and measured af-

ter constructing the graph. In general,  $P_t < P_s$  due to false heralding. A primary source of false heralding is when the emitter photon is not collected but the SPDC source produces two or more photon pairs that lead to a detection pattern, falsely signaling a successful swap. False heralding due to two signal photons is a well known and ubiquitous problem in entanglement swapping with photon pair sources based on nonlinear optics [33]. We can write an expression for the fidelity of the entanglement swapping procedure,  $P_t/P_s$ , using the known statistical distribution of entangled photon pairs produced via SPDC. Here, we assume photon number-resolved detection and perfect collection and detection of the signal photon once produced. This is because loss on that channel can generally be minimal and primarily affects the rate rather than the swapping fidelity (see Appendix D for the full calculation, including further experimental factors not discussed here). Furthermore, the intention here is to show that even quite low efficiency collection of the emitter photon can allow the generation of graph states. The probability of producing two entangled photon pairs is proportional to the square of the probability of producing a single entangled pair, and is controllable via the pump power of the SPDC (parameterized here by the quantity  $\xi$  [33]), thus introducing a tradeoff between rate and fidelity. The fidelity,  $F_{\text{swap}} = P_t/P_s$ , is given by

$$P_t(\eta_e, \xi) = \eta_e (1 - \xi)^2 \xi, \tag{2a}$$

$$P_s(\eta_e, \xi) = \left[\eta_e \xi + (1 - \eta_e) \xi^2\right] (1 - \xi)^2,$$
 (2b)

$$F_{\text{swap}}(\eta_e, \xi) = \frac{\eta_e}{\eta_e + (1 - \eta_e)\xi}.$$
 (2c)

In the absence of decoherence of the spins, we could simply work at  $\xi \ll 1$  (very low pair generation rate) to reduce the false heralding and increase the overall fidelity. However, this slows the rate of the graph production and introduces infidelity due to decoherence of the auxiliary spin(s). Given a set of experimental parameters, the rate of pair production can be optimized by tuning  $\xi$  to maximize the overall fidelity of the desired graph state, balancing the infidelity due to false heralds against the decoherence.

We present a simple example comparing these additional sources of infidelity to the limits set by spin-spin entangling gates and initial entanglement fidelities, for the case of constructing a graph state on a single auxiliary spin. Figure 4 depicts these estimates over a few regimes. The combined effect of false heralds and decoherence (blue) set the fidelity as

$$F(n_p, \eta_e, \xi) = F_{\text{swap}}(\eta_e, \xi)^{n_p} F_D^{(e)}(n_p) \times \langle F_D^{(s)}(n_p, P_s(\eta_e, \xi)) \rangle, \quad (3)$$

which we optimize over  $\xi$ , for fixed  $n_p$  and  $\eta_e$ . When only limited by decoherence (yellow), we can employ Equation (3), except now fixing  $F_{\text{swap}}(\eta_e, \xi) = 1$  and removing the need to optimize the fidelity. These estimates are applicable when constructing large star graph

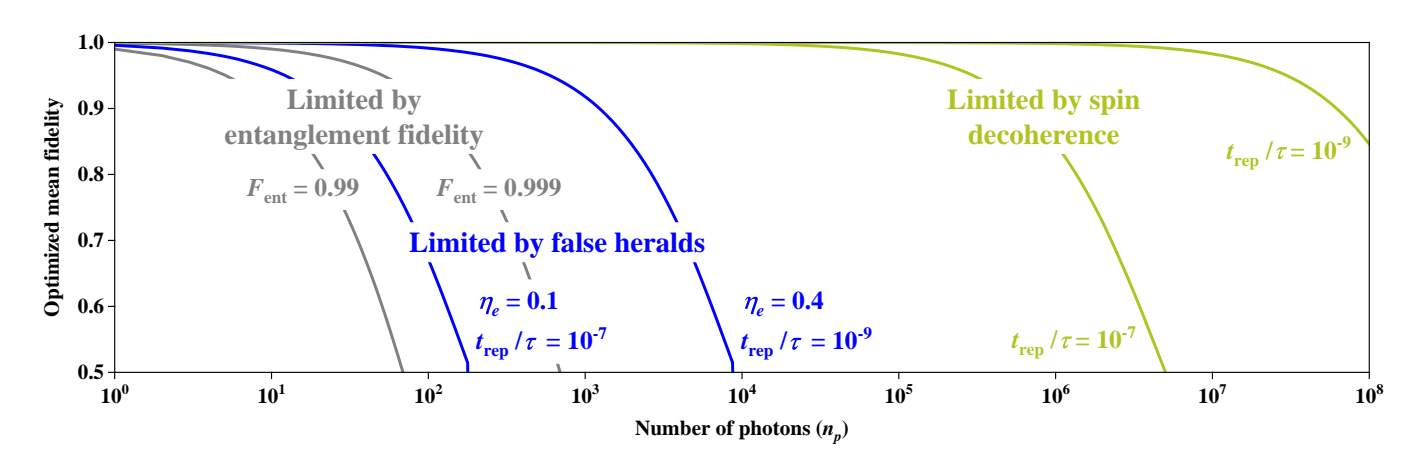


FIG. 4. Graph state fidelity versus photon number  $(n_p)$  for several different regimes of operations, and variable emitter-photon collection efficiencies  $(\eta_e)$  and dephasing timescales  $(t_{\rm rep}/\tau)$ . Gate and pair generation fidelities (grey) exponentially preclude the construction of large graph states in any scheme utilizing our "emit then add" method. With sufficient error correction or purification around these fidelities, regimes limited by false heralds and decoherence (blue) and decoherence alone (yellow), allow for the construction of significantly larger graph states.

states—the local-unitary equivalent to a Greenberger-Horne-Zeilinger (GHZ) state—and 1D cluster states.

## V. REALIZING SECURE TWO-PARTY COMPUTATION

As one application of our HoD scheme, we describe a method for securely computing an arbitrary Boolean function  $f:\{0,1\}^{\times n}\to\{0,1\}$  of either two parties or a restricted class of multi-party functions. As a special type of MBQC, our protocol performs the calculation through a sequence of measurements on distributed graph states. Only Pauli measurements are needed and the protocol can be implemented using the HoD method, for which the generation of the requisite resource state happens in parallel with the computation and no photonic memory is required.

Secure multi-party computation (MPC) is a task in which two or more parties compute some function on their individually held variables without revealing the values of the variables to each other [45, 46]. For example, in Yao's famous millionaire problem, two parties want to determine whose bank account has the most money without actually revealing how much money is in each account. MPC is a deeply-studied topic in both classical and quantum cryptography, and a variety of MPC protocols have been proposed achieving different levels of security and relying on different operational assumptions [47]. We propose an unconditionally secure method for restricted MPC that includes all two-party computations and requires only two rounds of public communication regardless of the size of the computational input. Our scheme follows a well-known approach of decomposing an MPC into "offline" and "online" phases [48–50]. In the offline phase, some universal computational resource is distributed to all the parties. Crucially, this resource

does not depend on the particular function being computed other than its input size. Then in the online phase this resource is used to compute some chosen function of the parties' inputs. For example, in the classical setting one well-known computational resource is a special form of shared randomness known as "Beaver triples," which can be used to efficiently compute logical AND gates in the online phase [51]. The problem of MPC then reduces to secure and efficient methods for distributing Beaver triples in the offline phase. In a similar spirit, our protocol involves distributing certain quantum graph states in the offline phase which then enable the computation of a logical AND in the online phase. Beyond its relatively low communication costs, a significant advantage of our protocol is that the parties can, in principle, use self-testing methods to verify that some untrusted source is faithfully distributing the correct graph state [52, 53], an ability that does not exist for classical shared randomness.

Suppose that N parties  $\mathbf{P}_1, \mathbf{P}_2, \dots, \mathbf{P}_N$  wish to compute some Boolean function  $f(\mathbf{x}_1, \dots, \mathbf{x}_N)$ , where  $\mathbf{x}_i$  is a string of bits representing the input for party i. In addition to correctness, the evaluation of f should be done securely such that the parties learn no more information about the individual  $\mathbf{x}_1, \dots, \mathbf{x}_N$  beyond their own input and what is revealed in the function value  $f(\mathbf{x}_1, \dots, \mathbf{x}_N)$ . To achieve this task, we propose a method of delegated computation in which a non-collaborating Referee is introduced to assist in the computation of  $f(\mathbf{x}_1, \dots, \mathbf{x}_N)$ . To maintain privacy, the Referee also should not learn any more information about the  $\mathbf{x}_i$  beyond what is implied by the computed value  $f(\mathbf{x}_1, \dots, \mathbf{x}_N)$ , nor does the Referee reveal any more information to the other parties than this value.

The protocol uses the fact that every Boolean function f can be expressed in an algebraic normal form (ANF), which presents f as a sum (mod 2) of different vari-

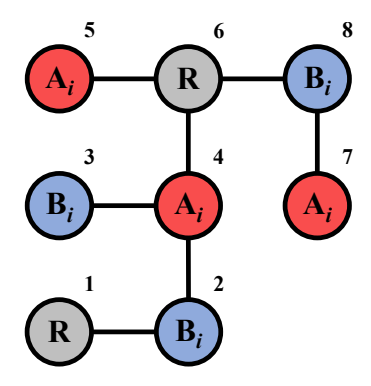


FIG. 5. In Stage I, each computation of a padded AND,  $b_i = x_i y_i + p_i$ , is accomplished using a graph state  $|G_I\rangle$  of this form. The qubits are distributed to parties  $\mathbf{A}_i$  (Alice),  $\mathbf{B}_i$  (Bob), and  $\mathbf{R}$  (the Referee) as shown. The numeric script k above each qubit reflects an example photon emission order.

able conjunctions. That is, we can write  $f = \sum_{i=1}^{\Re} c_i$ , where each  $c_i$  is the logical AND of a certain group of input variables. By combining variables belonging to the same party, every  $c_i$  becomes the conjunction of at most N variables, each one belonging to a different party. In this work, we restrict attention to functions f that admit an ANF whose conjunctions involve no more than two variables. This covers the entire class of two-party functions, but also includes certain multiparty functions, such as the three-party majority function  $\varphi_3(x,y,z) = xy + xz + yz \mod 2$ , which outputs the majority value among inputs  $x, y, z \in \{0, 1\}$ . In general, the functions we consider have the form f = $\sum_{i=1}^{\Re_1} x_i y_i + \sum_{i=1}^N z_i$ , which is separated into linear and quadratic parts. By again combining variables, we can assume that  $z_i$  is held by party  $\mathbf{P}_i$  and computed from her input  $\mathbf{x}_i$ . Furthermore, if each  $\mathbf{x}_i$  is no more than Mbits, then  $\Re_1 \leq {N \choose 2} M^2$ .

The protocol involves performing Pauli observables, X, Y, Z, on two types of graph states,  $|G_I\rangle$  and  $|G_{II}\rangle$ , depicted in Figures 5 and 6, respectively. The distribution of these states is conducted during the offline phase of the protocol. In practice, the states can be generated by some untrusted quantum source, and their correctness can be certified using self-testing methods (see Appendix B 4). Specific steps for building both  $|G_I\rangle$  and  $|G_{II}\rangle$  using a quantum emitter is presented in Appendix C 2. We note that the nontrivial emission order on  $|G_I\rangle$  set by our MPC requires two auxiliary spins to produce [32]. The online phase of the protocol then involves specific sequences of Pauli measurements and public communication, and these sequences take place in two different stages

Stage I uses  $|G_I\rangle$  to compute the bit values

$$b_i = x_i y_i + p_i, \qquad i = 1, \cdots, \mathfrak{R}_1, \tag{4}$$

where each  $p_i$  is an independent one-time pad bit that is

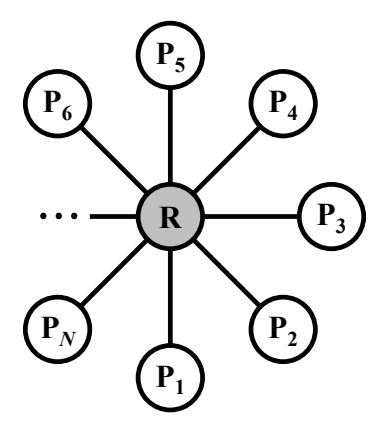


FIG. 6. The graph state  $|G_{\text{II}}\rangle$  used to compute values p in Stage II. The numeric subscript labels both the party  $\mathbf{P}_k$  and an example photon emission ordering. In total,  $n_p = N + 1$  photons are required for the N parties and the Referee.

private from all the parties, including the Referee.

**Stage I.** Input: Parties  $A_i$  (Alice) and  $B_i$  (Bob) input bits  $x_i$  and  $y_i$ , respectively.

- 1. The Referee and Bob measure X and Z on qubits 1 and 2, respectively, obtaining a common measurement outcome  $s = m_1 = m_2$ .
- 2. Bob measures Z on qubit 3, obtaining  $m_3$ . He announces  $\delta_i = y_i + m_3$ . Alice then applies  $Z^{\delta_i}$  to qubit 4.
- 3. Alice measures  $W^{x_i}Z(W^{\dagger})^{x_i}$  on qubits 4 and 5, where  $W \equiv (iX)^{1/2}$ , computing  $\alpha_i = x_i + m_4 + m_5$  from her outcomes. Note that  $WZW^{\dagger} = Y$ .
- 4. The Referee measures  $V^s X(V^{\dagger})^s$  on qubit 6, where  $V \equiv (-iZ)^{1/2}$ , obtaining  $b_i = m_6$ . Note that  $VXV^{\dagger} = Y$ .
- 5. Alice measures Z on qubit 7, obtaining  $m_7$ . She announces  $\gamma_i = x_i + m_7$ . Bob then applies  $Z^{\gamma_i}$  to qubit 8.
- 6. Bob measure  $W^s Z(W^{\dagger})^s$  on qubit 8 obtaining  $\beta_i = m_8$ .

As shown in Appendix B 1, the Referee's measurement outcome in step 4. satisfies  $b_i = x_i y_i + p_i$ , where  $p_i = \alpha_i + \beta_i$ . The above sequence is repeated on a fresh copy of  $|G_I\rangle$  for each  $i = 1, \dots, \mathfrak{R}_1$ , with the values of  $\alpha_i$  and  $\beta_i$  possibly being obtained by different parties in each iteration. Note that if the Referee added all the  $b_i$  at the end of Stage I, the computed value would be

$$\sum_{i=1}^{\mathfrak{R}_1} b_i = f + \sum_{i=1}^{N} z_i + \sum_{i=1}^{\mathfrak{R}_1} (\alpha_i + \beta_i) = f + \sum_{i=1}^{N} \mu_i, \quad (5)$$

where  $\mu_i$  denotes the sum of the variables in the set  $\{\alpha_i, \beta_i\}_{i=1}^{\Re_1} \cup \{z_i\}_{i=1}^N$  belonging to party *i*. Stage II then amounts to removing the term  $\sum_{i=1}^N \mu_i$  from the RHS of Equation (5).

Stage II is performed using an (N+1)-party GHZ state  $|G_{II}\rangle$  (see Figure 6) shared between the Referee and the N parties. The following steps are then taken.

**Stage II.** Input: Parties  $\mathbf{P}_i$  input their respective bits  $\{\mu_i\}_{i=1}^N$  obtained from the set  $\{\alpha_i, \beta_i\}_{i=1}^{\mathfrak{R}_1} \cup \{z_i\}_{i=1}^N$ , as in Equation (5). The Referee inputs  $\{b_i\}_{i=1}^{\mathfrak{R}_1}$  obtained from Stage I.

- 1. Party  $\mathbf{P}_k$  measures Z on qubit k for qubits  $1, \dots, N$ . She then announces  $\nu_k = \mu_k + m_k$ .
- 2. The Referee measures X to learn  $\sum_{k=1}^{N} m_k$  and then adds this to  $\sum_{k=1}^{N} \nu_k$  to obtain  $\sum_{k=1}^{N} \mu_k$ . The latter is then added to the sum  $\sum_{i=1}^{\Re_1} b_i$  to obtain f, which is then announced to all the parties.

It should be noted that by parallelization, both Stages I and II can be performed using just two rounds of simultaneous communication. Indeed, each party needs to broadcast at most two public messages, the first being no more than  $\log \mathfrak{R}_1$  bits, and the second being one bit. When run in parallel, all the Stage I messages can be broadcast concurrently, and likewise for the Stage II messages.

Intuitively, this protocol is secure due to the one-time pad bits that are generated with each measurement on the graph states. While there are a variety of different approaches to defining security in multipartite computation, in this work we demand as a security condition that playing honestly does not reveal any more information about one's input than what can be inferred from the final function output. We prove in Appendix B 3 that our protocol satisfies this condition.

**Performance.** To handle experimental errors in the above protocol, we can employ a simple repetition code to suppress the effects of any infidelity in our ability to make  $|G_I\rangle$  and  $|G_{II}\rangle$  on the output of the computation f. By determining the total bit error probability when computing each  $b_i$  in Stage I and p in Stage II, an arbitrarily small total bit error probability  $\epsilon_f$  on the computation output f can be chosen to set the number of repetitions required for each Stage I and II, respectively. We use this information to estimate the lower bound rate of computation at which N parties can compute f on their M-bit inputs. Details are proved in Appendix B 2.

Functionally, our protocol allows for the secure implementation of any two-party Boolean function, f, by repeatedly generating and distributing copies of the 8-qubit state  $|G_I\rangle$  and then generating and distributing one copy of  $|G_{II}\rangle$  (which is simply a 3-qubit GHZ state). The number of required copies of  $|G_I\rangle$  depends (polynomially) on the size of the input, M, and the desired final error probability,  $\epsilon_f$ . We re-emphasize here that this can be done

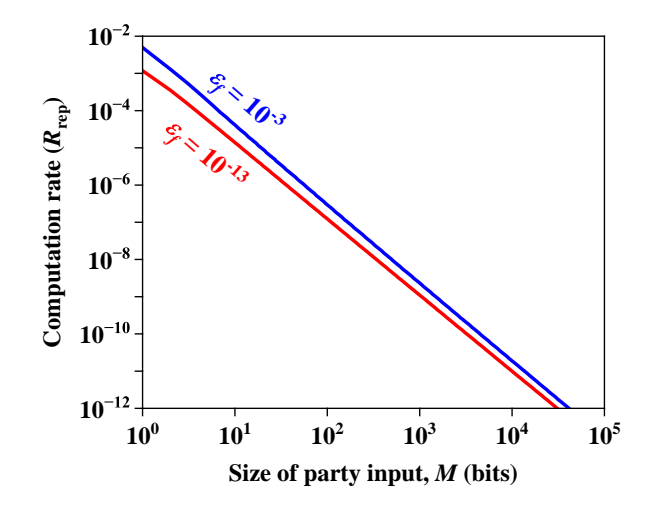


FIG. 7. Error corrected two-party computation rate versus the number of input bits to f using the HoD scheme, shown for two acceptable error probabilities on the computation  $(\epsilon_f)$ . The rate is expressed in units of the repetition rate of excitation of the chosen quantum emitter,  $R_{\rm rep}$ , which is typically in the range of  $10^6-10^9~{\rm s}^{-1}$  for highly coherent emitters. The individual bit error probabilities for Stage I and Stage II, respectively, are 0.008 and 0.003, assuming  $\eta_e=0.4$ ,  $F_{\rm ent}=0.999$ , and  $t_{\rm rep}/\tau=10^{-9}$  (see. Appendix D for details). We see that these parameters allow virtually unlimited reduction in the total error probability with minimal change in the overall rate.

with one emitter and two auxiliary spins, and the spins need only remain coherent for the time to make each copy of  $|G_I\rangle$ , a requirement easily met with current trapped ion or atom array systems. Using the fidelity estimates established in Section IV and detailed in Appendix D, we can conservatively estimate the maximum possible bit error probability in either Stage from the compliment of the probability that no bit error occurs, that is, the probability to successfully generate  $|G_I\rangle$  and  $|G_{II}\rangle$  in our proposed HoD scheme. In Figure 7, we plot the lower bound rate of computation (which is proportional to the number of copies of  $|G_I\rangle$  that are required) at which our protocol can operate with error correction, in units of  $R_{\rm rep}$ , against the size of each parties input, M, for total acceptable error probabilities  $\epsilon_f = \{10^{-3}, 10^{-13}\}$ .

# VI. DISCUSSION AND CONCLUSION

The schemes introduced here naturally lend themselves to various extensions and modifications to increase functionality. First, combining with a high degree of multiplexing, such as between many arrays of atoms or ions, would increase the generation rate with a linear factor in the degree of multiplexing. Incorporating this with heralding means that photons can be routed upon successful generation of spin-photon entanglement. Another

extension is the opportunity for substantial spectral engineering of the idler photon in the HoS scheme. As mentioned above, the idler photon can be produced at virtually any arbitrary wavelength regardless of the emission wavelength of the emitting spin, including using a superconducting qubit as the spin and generating a signal-idler pair with a microwave signal and an optical idler [54]. We also point out that the bandwidth of the idler photon can be different than the typically narrow and fixed bandwidth of the emitter. Filtering, time lensing [55], and/or source engineering [22, 56] can enable substantial broadening or narrowing of the idler photon compared to the emitter photon.

In this work, we have demonstrated the feasibility of generating photonic graph states with inefficient quantum emitters and give a central example of its applications to secure multi-party computation. Significantly, our schemes offer polynomial scaling in the time to construct graph states of hundreds of photons with high fidelity on current generation trapped ion experiments [12, 13], even when the collection efficiency of emitter

photons is poor. The "emit then add" approach requires additional resource costs for making graph states, but we show that it is feasible with current and near-term experimental hardware. Our scheme is a toolbox for making large entangled photonic states for MBQC and other applications that are limited by spin decoherence rather than photon collection efficiency. We specifically show an application to realize distributed multi-party computation that is feasible in the near-term with current hardware.

#### ACKNOWLEDGMENTS

We acknowledge helpful discussions with Kejie Fang and Vito Scarola. E.C. thanks Christian Schaffner for some helpful explanations on multi-party computation. This work was supported by the NSF Quantum Leap Challenge Institute on Hybrid Quantum Architectures and Networks (NSF Award No. 2016136).

## Appendix A: Preliminaries on graph states

For an arbitrary graph G = (V, E) with vertices  $V = \{a_1, \dots, a_n\}$  and edge set  $E \subset V \times V$ , consider the *n*-qubit operator obtained by performing a controlled -Z gate,  $CZ_{a,b}$ , between every  $(a,b) \in E$ . We denote this global operator by

$$U_G = \prod_{(a,b)\in E} CZ_{a,b}.$$
 (A1)

The graph state associated with the graph G is the n-qubit state

$$|G\rangle = U_G |+\rangle^{\otimes V}. \tag{A2}$$

Note that  $|+\rangle^{\otimes n}$  is stabilized by n commuting operators  $\{X_a\}_{a\in V}$ . Hence the stabilizer of  $|G\rangle$  can be understood by examining the how the  $X_a$  transform under  $U_G$ . Since  $CZ_{a,b}(X_a)CZ_{a,b}=X_aZ_b$ , it follows that the stabilizer of  $|G\rangle$  is generated by the operators  $\{K_a\}_{a\in V}$ , where

$$K_{a} = U_{G}X_{a}U_{G}$$

$$= X_{a} \prod_{b \in N_{a}} Z_{b}$$

$$= X_{a} \prod_{b \in V} Z_{b}^{\Gamma_{a,b}} \qquad \forall a \in V,$$
(A3)

and  $\Gamma$  is the adjacency matrix of G.

For any n-qubit graph state  $|G\rangle$ , we can generate an orthonormal basis for  $\mathbb{C}_2^N$ , called the associated graph basis. The basis vectors have the form

$$Z^{\mathbf{r}}|G\rangle$$
 where  $Z^{\mathbf{r}} := Z_1^{r_1} \otimes Z_2^{r_2} \otimes \cdots \otimes Z_N^{r_N}$ , (A4)

and we will call  $\mathbf{r} = (r_1, r_2, \dots, r_n) \in \mathbb{Z}_2^n$  a conditional phase vector and each bit  $r_k$  phase information for qubit k. To see that these states are orthogonal, let  $\mathbf{r}$  and  $\mathbf{r}'$  be two distinct conditional phase vectors, and suppose their bit values differ in position a. Then  $K_a$  will anti-commute with  $Z^{\mathbf{r}}Z^{\mathbf{r}'}$ , and so

$$\langle G|Z^{\mathbf{r}}Z^{\mathbf{r}'}|G\rangle = \langle G|Z^{\mathbf{r}}Z^{\mathbf{r}'}K_a|G\rangle = -\langle G|K_aZ^{\mathbf{r}}Z^{\mathbf{r}'}|G\rangle = -\langle G|Z^{\mathbf{r}}Z^{\mathbf{r}'}|G\rangle. \tag{A5}$$

We will be particularly interested in how the graph basis states transform under the local Pauli measurements of Y and Z. For a binary vector  $\mathbf{r} \in \mathbb{Z}_2^n$  and subset of nodes  $S \subset V$ , let  $\mathbf{r} - S$  denote the vector of length n - |S|obtained from **r** by removing the coordinates in S. Suppose that for an initial graph basis state  $Z^{\mathbf{r}}|G\rangle$ , either Y or Z is measured on qubit a and outcome  $m_a \in \{0,1\}$  is received. The initial state transforms as follows:

$$Z_a: Z^{\mathbf{r}}|G\rangle \mapsto \left(\prod_{b\in N_a} Z_b^{m_a}\right) Z^{\mathbf{r}-a}|G-a\rangle,$$
 (A6a)

$$Y_a: \qquad Z^{\mathbf{r}}|G\rangle \mapsto \left(\prod_{b\in N_a} \left(-iZ_b\right)^{1/2} Z_b^{r_a+m_a}\right) Z^{\mathbf{r}-a} \left|\tau_a(G) - a\right\rangle, \tag{A6b}$$

where  $\tau_a(G)$  is the local complementation of G at vertex a, i.e.  $\tau_a(G)$  is the graph  $(V, E\Delta E(N_a, N_a))$ , and  $\tau_a(G) - a$ is the graph obtained by removing a from  $\tau_a(G)$  [57]. Explicitly,

$$|\tau_a(G)\rangle = (-iX_a)^{1/2} \left( \prod_{b \in N_a} (iZ_b)^{1/2} \right) |G\rangle, \tag{A7}$$

describes a set of single-qubit rotations comprising a local complementation. Note that the  $Y_a$  post-measurement state can always be transformed back to the associated graph basis by performing  $(iZ_b)^{1/2}$  on each  $b \in N_a$ . For the special case of measurement at a leaf in the graph, a vertex with only a single neighbor such that  $\tau_a(G) = G$ , the  $Y_a$ post-measurement state after rotation back to the graph basis is effectively a  $Z_a$  post-measurement state up to the conditional phase flip  $Z_b^{r_a}$ .

## Phase transmission along a chain

Consider the effect of locally measuring along some linear chain in graph G. Let  $a_1, a_2, a_3, \dots, a_n, a_{n+1}$  denote the constituent qubits, with  $a_1$  being the first node in the chain and  $a_{n+1}$  being the final node, which is connected to the remainder of the graph and left unmeasured in this sub-routine. The specific measurement sequence consists of measuring Y on  $a_1$  and  $(-iZ)^{1/2}Y(iZ)^{1/2} = -X$  on  $a_k$  for all  $k = 2, \dots, n-1$ . If the total state prior to measurement is a graph basis state  $Z^{\mathbf{r}}|G\rangle$  and  $(m_{a_1}, \cdots, m_{a_{n-1}})$  is the binary sequence of outcomes from these measurements, then by Equation (A6b) the overall state evolution is

$$Y_{a_1}, (-X_{a_2}), \cdots, (-X_{a_{n-1}}): Z^{\mathbf{r}} | G \rangle \mapsto [-iZ_{a_n}]^{1/2} Z_{a_n}^{\Omega} Z^{\mathbf{r} - \{a_1, \cdots, a_{n-1}\}} | G - \{a_1, \cdots, a_{n-1}\} \rangle,$$
 (A8)

where  $\Omega = \sum_{i=1}^{n-1} (r_{a_i} + m_{a_i}) \mod 2$ . Crucially, each  $m_{a_k}$  is a random bit uncorrelated from  $\mathbf{r}$  and any other measurement data. Hence, we can think of each  $m_{a_k}$  as a one-time pad that is added to the conditional phase information  $r_{a_k}$  when passing from node  $a_k$  to  $a_{k+1}$ .

#### Phase transmission at a fork

Consider the effect of measuring two qubits, a and b, that are connected to a single common node c. Suppose the total state prior to measurement is a graph basis state  $Z^r |G\rangle$ . If  $m_a$  and  $m_b$  denote the binary outcomes when either Y or Z is measured on both qubits, the respective state transformations are given by

$$Y_{a}, Y_{b}: Z^{\mathbf{r}} | G \rangle \mapsto Z_{c}^{r_{a}+r_{b}+1} Z_{c}^{m_{a}+m_{b}} Z^{\mathbf{r}-\{a,b\}} | G - \{a,b\} \rangle,$$

$$Z_{a}, Z_{b}: Z^{\mathbf{r}} | G \rangle \mapsto Z_{c}^{m_{a}+m_{b}} Z^{\mathbf{r}-\{a,b\}} | G - \{a,b\} \rangle,$$
(A9a)
$$(A9b)$$

$$Z_a, Z_b: Z^{\mathbf{r}} | G \rangle \mapsto Z_c^{\mathbf{m}_a + m_b} Z^{\mathbf{r} - \{a,b\}} | G - \{a,b\} \rangle,$$
 (A9b)

up to an overall phase. Hence, the key difference between the two measurements is that  $Y_a, Y_b$  transfers the conditional phase flip  $Z_c^{r_a+r_b+1}$  onto the state  $|G - \{a,b\}\rangle$  while  $Z_a, Z_b$  does not.

#### Appendix B: Secure multi-party computation

We verify correctness and prove security of our multi-party computation protocol detailed in Section V, using the preliminaries of Appendix A. The measurement sequences described in Stages 1 and 2 together accomplish the computation of any Boolean function up to quadratic order in the parties' inputs. We verify these sequences by tracing through the transformation of the graph states  $|G_I\rangle$  and  $|G_{II}\rangle$  used in each part of the protocol, and the information that is transmitted along the graph in the form of phase flips conditioned on both the parties' inputs and their measurements. Subsequently, we detail how classical error correction can be utilized to suppress a bit error on the output of the computation. We establish security by demonstrating that the classically communicated information in the protocol reveals no new information to any of the other parties about their input, other than what they would learn from the final output of the computation. Finally, we discuss how self-testing can be employed to further secure against a possibly corrupt Source.

## 1. Correctness

To verify correctness for the computation of f, we track the evolution of phase information as defined in Appendix A through both Stages of the protocol. A graph state  $|G\rangle$  consisting of n qubits, labeled  $1, \dots, n$ , is initialized. We denote  $\mathbf{m} = (m_1, \dots, m_n)$  as the binary vector of measurement outcomes for each of the qubits. In general, measurements change the shape of the graph disconnecting the measured qubit and applying conditional phase flips on its neighbors. As the labeling we assigned represents a possible photon emission ordering for generating the graph state in a quantum emitter-based experimental scheme, it is convenient to keep this labeling for each qubit despite transformations in the graph induced by the measurement sequence.

a. Stage I

Stage I details the measurement sequence performed on  $|G_I\rangle$ , requisite for computing each  $b_i = x_i y_i + p_i$ . Let  $x_i$  and  $y_i$  be the input for the parties  $\mathbf{A}_i$  and  $\mathbf{B}_i$ , respectively. We will refer to  $\mathbf{A}_i$  and  $\mathbf{B}_i$  as Alice and Bob, although in general these labels change for different  $i \in \{1, 2, \dots, \mathfrak{R}_1\}$ . The measurement outcome  $m_k$  denotes the measurement m of the k<sup>th</sup> qubit in the 8-qubit graph state, depicted in Figure 5. For simplicity, we suppress any additional subscript denoting the iteration of Stage I and reset these labels with each new copy of  $|G_I\rangle$ .

In step (1.), the Referee's X measurement on qubit 1 decouples Bob's qubit 2 from the rest of the graph. This leads to correlated outcomes  $s=m_1=m_2$  as the parties are each measuring an independent component of the generator  $X_1Z_2$  that stabilizes the state. From Equation (A6a) and Equation (A8), we see this adds the conditional phase flip  $Z_4^m$  to Alice's qubit. In step (2.), Bob's measurement of qubit 3 introduces a conditional phase flip  $Z_4^{m_3}$  on Alice's qubit. Her subsequent rotation of the qubit, using Bob's announced  $\delta_i=y_i+m_3$ , transforms the state such that the total conditional phase on her qubit is described by  $Z_4^{y_i+s}$ . Alice then in step (3.) performs a measurement at a fork on qubits 4 and 5, conditioned on her own input  $x_i$ , and obtains  $\alpha_i=x_i+m_4+m_5$ . From Equation (A9a) and Equation (A9b), we see that the total conditional phase applied to the Referee's qubit 6 from this step is  $Z_6^{x_i(y_i+s+1)+m_4+m_5}=Z_6^{x_i(y_i+s+)+\alpha_i}$ . In steps (4.) and (6.), the pad s informs the Referee and Bob the correct basis to measure their respective qubits, in order to obtain a correlated outcome. In more detail, the parties each measure their independent component of the generator  $X_6Z_8$  or  $Y_6Y_8$ , conditioned on whether s=0 or s=1, respectively. Note that if s=0 the Referee's measurement in step (4.) decouples the remaining two qubits, shared between Alice and Bob, and leaves Bob's qubit invariant under the action of step (5.) That is, the combined action of Alice and Bob in step (5.) produces a conditional phase  $Z_8^{x_i}$  on Bob's qubit. Hence, step (6.) produces a correlated outcome between the parties' measurements and prior phase information such that

$$(x_i(y_i+s) + \alpha_i) + b_i + (sx_i) + \beta_i = 0.$$
 (B1)

where we denote  $b_i = m_6$  belonging to the Referee and  $\beta_i = m_8$  belonging to Bob, and the Referee obtains

$$b_i = x_i y_i + p_i$$
 (where  $p_i = \alpha_i + \beta_i$ ), (B2)

as desired.

b. Stage II

Correctness is proved for Stage II in the same way as before, where now each party is labeled by a  $\mathbf{P}_k$ , for  $k = 1, \dots, N$ . We again let  $\mathbf{m} = (m_1, \dots, m_N, m_R)$  represent the binary vector of measurement outcomes from each party on the N + 1-qubit graph state, depicted in Figure 6. We note that the ordering of the labels need not be

tied to a particular photon emission ordering, as all the measurements performed commute with each other and all classically communicated information need only be shared after each party's measurement.

We first recognize that each party is measuring an independent component of the generator,  $X_R Z_1 \cdots Z_N$ , of this graph state. This implies for the Referee's outcome  $m_R$  that

$$m_{\rm R} + \sum_{k=1}^{N} m_k = 0.$$
 (B3)

This is equivalent to the notion that the measurement of each party  $\mathbf{P}_k$  in step (1.) introduces a conditional phase flip  $Z^{m_k}$  on the Referee's qubit, such that total action on the Referee's qubit is  $\prod_k Z^{m_k}$ . The Referee can determine the value of p by adding their outcome  $m_k$  to the sum of the party's announced  $\nu_k = \mu_k + m_k$ , such that

$$p = m_{R} + \sum_{k=1}^{N} \nu_{k} = \sum_{i=1}^{\mathfrak{R}_{1}} (\alpha_{i} + \beta_{i}) + \sum_{k=0}^{\mathfrak{R}_{2}} z_{i},$$
 (B4)

and the output of the computation is achieved:

$$f = p + \sum_{i=1}^{\mathfrak{R}_1} b_i = \sum_{i=1}^{\mathfrak{R}_1} x_i y_i + \sum_{i=1}^{\mathfrak{R}_2} z_i.$$
 (B5)

# 2. Including Error Correction

In practice, each bit conjunction computed in Stage I of the protocol as well as the final summation computed in Stage II will have some error. In this section we describe a basic error correction method that can be employed to suppress the overall computational error as much as desired.

Let  $\epsilon_*$  denote the largest probability of a bit error in each iteration of Stage I, and let  $\Xi_i$  be the indicator variable for the occurrence of an error in iteration i. Thus, while the noiseless protocol generates bit value  $b_i = x_i y_i + p_i$  in iteration i, the actual implementation generates bit values

$$b_i = x_i y_i + p_i + \Xi_i. \tag{B6}$$

To deal with this, the Referee can employ a simple repetition code. That is, each iteration i is repeated  $K_I$  times, from which the Referee obtains values  $b_{(i,1)}, b_{(i,2)}, \cdots, b_{(i,K_I)}$ , where  $b_{(i,j)} = x_i y_i + p_{(i,j)} + \Xi_{(i,j)}$ . Recalling that  $p_{(i,j)} = \alpha_{(i,j)} + \beta_{(i,j)}$  is the sum of Alice and Bob's private bits, for each  $j = 2, \cdots, K_I$ , Alice and Bob announce to the Referee messages  $\alpha_{(i,1)} + \alpha_{(i,j)}$  and  $\beta_{(i,1)} + \beta_{(i,j)}$ , respectively. The Referee adds these to each corresponding  $b_{(i,j)}$  so that his  $K_I$  bit values have the form  $b_{(i,j)} = x_i y_i + p_i + \Xi_{(i,j)}$ , where  $p_i = \alpha_{(i,1)} + \beta_{(i,1)}$ . Note that each  $\alpha_{(i,j)}$  and  $\beta_{(i,j)}$  is an independent private random bit for Alice and Bob, so the announcements of  $\alpha_{(i,1)} + \alpha_{(i,j)}$  and  $\beta_{(i,1)} + \beta_{(i,j)}$  do not reveal any information about  $\alpha_{(i,1)}$  and  $\beta_{(i,1)}$ . The Referee then performs majority voting on the bit values  $b_{(i,j)}$ , accepting the value appearing the most among the  $K_I$  sub-iterations. By Hoeffding's inequality, this value will be  $b_i = x_i y_i + p_i$  with a bit error rate  $\delta \leq \exp\left[-2K_I(\frac{1}{2} - \epsilon_* - \frac{1}{2K_I})^2\right]$ . Then, the combined bit error rate in computing  $\sum_{i=1}^{\Re_1} b_i$  is equal to the probability that an odd number of bit errors occur among the  $b_i$ . A counting argument shows this probability to be

$$\epsilon_I = \frac{1}{2} [1 - (1 - 2\delta)^{\mathfrak{R}_1}] \le \delta \mathfrak{R}_1 \le \mathfrak{R}_1 \cdot \exp\left[-2K_I(\frac{1}{2} - \epsilon_* - \frac{1}{2K_I})^2\right].$$
 (B7)

Note that to suppress the bit error rate, the number of repetitions  $K_I$  needed for each iteration i is exponentially smaller than the total number of iterations  $\mathfrak{R}_1$ .

Moving to Stage II, there will be a separate bit error rate  $\epsilon_+$  in the Referee's computation of p using the state  $|G_{II}\rangle$ . Again, a repetition code can be used by repeating this step  $K_{II}$  times and achieving an overall bit error rate on p of  $\epsilon_{II} \leq \exp\left[-2K_{II}(\frac{1}{2}-\epsilon_+-\frac{1}{2K_{II}})^2\right]$ . Therefore, the total error rate in computing f is  $\epsilon_I + \epsilon_{II} - 2\epsilon_I\epsilon_{II}$ , which is exponentially small in the repetitions  $K_I$  and  $K_{II}$ . In particular, to obtain a bit error probability  $\epsilon_f$  on the computation of f for fixed  $\epsilon_*$  and  $\epsilon_+$ , it suffices to take

$$K_{I} = \left| \frac{1}{(\frac{1}{2} - \epsilon_{*})^{2}} \ln \sqrt{\frac{\mathfrak{R}_{1}}{\epsilon_{f}}} \right| \leq \left| \frac{1}{(\frac{1}{2} - \epsilon_{*})^{2}} \ln \left( \frac{MN}{\sqrt{2\epsilon_{f}}} \right) \right|,$$
 (B8a)

$$K_{II} = \left[ \frac{1}{(\frac{1}{2} - \epsilon_+)^2} \ln \sqrt{\frac{1}{\epsilon_f}} \right]. \tag{B8b}$$

In total, the N-party computation of f on each party's M-bit input can be implemented with error correction in our protocol at a lower bound unit rate of

$$\frac{R}{R_0} \ge \frac{MN}{4M^2N^2 \left\lceil \frac{\ln(MN/\sqrt{2\epsilon_f})}{\left(\frac{1}{2} - \epsilon_*\right)^2} \right\rceil + (N+1) \left\lceil \frac{\ln(1/\sqrt{\epsilon_f})}{\left(\frac{1}{2} - \epsilon_+\right)^2} \right\rceil},$$
(B9)

where  $R_0$  is the scheme-dependent average rate to add a new photon to a graph state. For the HoD scheme we propose,  $R_0 = \eta_e R_{\text{rep}}$ .

## 3. Security

Having established correctness of the proposed protocol, we now prove that it is secure under the requirements defined in Section V. Recall, we demand as a security condition that playing honestly does not reveal any more information about one's input than what can be inferred from the final function output. We will show that this is true under the assumption that the Referee does not collaborate with any of the parties by supplying them with side information.

In the first phase, each state  $|G_I\rangle^{\mathbf{A}_i\mathbf{B}_i\mathbf{R}}$  is a tripartite state, held by Alice, Bob, and the Referee. Suppose that Alice is playing honestly, and a dishonest Bob is trying to learn about her input based on his local quantum information and whatever Alice discloses in an honest execution of the protocol. The only information he obtains in Stage I is the public message  $\gamma_i = x_i + m_7$  announced by Alice. Hence, suppose that Alice's input is described by the random variable  $\mathbf{X}_i$  with values  $x_i$  having a prior distribution  $p(x_i)$ , which is known to all parties. Bob's initial state of knowledge of variable  $\mathbf{X}_i$  given his share of  $|G_I\rangle^{\mathbf{A}_i\mathbf{B}_i\mathbf{R}}$  is described by the density matrix

$$\sigma^{\mathbf{X}_i \mathbf{B}_i} = \sum_{x_i=0}^{1} p(x_i) |x_i\rangle \langle x_i|^{\mathbf{X}_i} \otimes \operatorname{tr}_{\mathbf{A}_i \mathbf{R}} \left( |G_I\rangle \langle G_I|^{\mathbf{A}_i \mathbf{B}_i \mathbf{R}} \right).$$
(B10)

After Alice's measurement and Bob's learning of the value  $\gamma_i$ , his updated state of knowledge conditioned on this new information is

$$\sigma_{\gamma_i}^{\mathbf{X}_i \mathbf{B}_i} = \sum_{x_i=0}^{1} \sum_{m_7=0}^{1} p(x_i, m_7 | \gamma_i) |x_i\rangle\langle x_i|^{\mathbf{X}_i} \otimes \operatorname{tr}_{\mathbf{A}_i \mathbf{R}} \left( |m_7\rangle\langle m_7|_7 |G_I\rangle\langle G_I|^{\mathbf{A}_i \mathbf{B}_i \mathbf{R}} \right) / p(m_7).$$
(B11)

A calculation shows that

$$\operatorname{tr}_{\mathbf{A}_{i}\mathbf{R}}\left(|m_{7}\rangle\langle m_{7}|_{7}|G_{I}\rangle\langle G_{I}|^{\mathbf{A}_{i}\mathbf{B}_{i}\mathbf{R}}\right) = \frac{\mathbb{I}_{2}}{2} \otimes \frac{\mathbb{I}_{3}}{2} \otimes \operatorname{tr}_{7}\left(|m_{7}\rangle\langle m_{7}|_{7} \frac{|+0\rangle\langle+0|_{78} + |-1\rangle\langle-1|_{78}}{2}\right)$$

$$= \frac{1}{2}\left(\frac{\mathbb{I}_{2}}{2} \otimes \frac{\mathbb{I}_{3}}{2} \otimes \frac{\mathbb{I}_{8}}{2}\right)$$

$$= \frac{1}{2}\operatorname{tr}_{\mathbf{A}_{i}\mathbf{R}}\left(|G_{I}\rangle\langle G_{I}|^{\mathbf{A}_{i}\mathbf{B}_{i}\mathbf{R}}\right). \tag{B12}$$

In other words, the post-measurement state of Bob's subsystem is independent of Alice's measurement outcome. Since  $m_7$  is a uniform random bit independent of  $x_i$ , we have  $p(m_7) = \frac{1}{2}$  and  $p(x_i|\gamma_i) = p(x_i)$ . Thus,

$$\sigma_{\gamma_{i}}^{\mathbf{X}_{i}\mathbf{B}_{i}} = \sum_{x_{i}=0}^{1} \sum_{m_{i}=0}^{1} p(x_{i}, m_{7}|\gamma_{i}) |x_{i}\rangle\langle x_{i}|^{\mathbf{X}_{i}} \otimes \operatorname{tr}_{\mathbf{A}_{i}\mathbf{R}} \left( |G_{I}\rangle\langle G_{I}|^{\mathbf{A}_{i}\mathbf{B}_{i}\mathbf{R}} \right)$$

$$= \sum_{x_{i}=0}^{1} p(x_{i}) |x_{i}\rangle\langle x_{i}|^{\mathbf{X}_{i}} \otimes \operatorname{tr}_{\mathbf{A}_{i}\mathbf{R}} \left( |G_{I}\rangle\langle G_{I}|^{\mathbf{A}_{i}\mathbf{B}_{i}\mathbf{R}} \right)$$

$$= \sigma^{\mathbf{X}_{i}\mathbf{B}_{i}}.$$
(B13)

This shows that Bob's knowledge of Alice's input does not change throughout the course of Stage I. The same is also clearly true for Stage II since the  $\operatorname{tr}_{\mathbf{R}}|G_{II}\rangle\langle G_{II}|=\frac{1}{2}(|+\cdots+\rangle\langle+\cdots+|+|-\cdots-\rangle\langle-\cdots-|)$ , and so the measurement outcomes  $m_k$  of the honest parties  $\mathbf{P}_k$  measuring Z are independent of each other and of the values  $\mu_k$ . Therefore,

the only new information Bob learns about Alice's input comes through the announcement of  $f(\mathbf{x}_1, \dots, \mathbf{x}_N)$  by the Referee at the end of the protocol. A similar conclusion is reached in the scenario of an honest Bob and a dishonest

Now we consider the Referee. Since there is no collusion with parties  $\mathbf{P}_1, \dots, \mathbf{P}_k$ , from the Referee's perspective, either all parties are playing fairly or some are acting maliciously; in the latter case, it is unknown who these parties are or what attacks they are employing. Therefore, a corrupt Referee wanting to learn the inputs of one or more honest parties should proceed by assuming that all parties are playing honestly. Like before, in each iteration of  $|G_I\rangle^{\mathbf{A}_i\mathbf{B}_i\mathbf{R}}$ , the Referee's initial state and description of the variables  $\mathbf{X}_i$  and  $\mathbf{Y}_i$  is given by

$$\sigma^{\mathbf{X}_{i}\mathbf{Y}_{i}\mathbf{R}} = \sum_{x_{i}, y_{i}=0}^{1} p(x_{i})p(y_{i}) |x_{i}\rangle\langle x_{i}|^{\mathbf{X}_{i}} \otimes |y_{i}\rangle\langle y_{i}|^{\mathbf{Y}_{i}} \otimes \operatorname{tr}_{\mathbf{A}_{i}\mathbf{B}_{i}} \left(|G_{I}\rangle\langle G_{I}|^{\mathbf{A}_{i}\mathbf{B}_{i}\mathbf{R}}\right).$$
(B14)

Note that tracing out qubits 2, 4, 5, and 8 completely dephases all the remaining qubits in  $|G_I\rangle$ :

$$\operatorname{tr}_{2,4,5,8}\left(|G_I\rangle\langle G_I|^{\mathbf{A}_i\mathbf{B}_i\mathbf{R}}\right) = \frac{\mathbb{I}_1}{2} \otimes \frac{\mathbb{I}_3}{2} \otimes \frac{\mathbb{I}_6}{2} \otimes \frac{\mathbb{I}_7}{2}. \tag{B15}$$

Hence,

$$\operatorname{tr}_{\mathbf{A}_{i}\mathbf{B}_{i}}\left(|m_{3}\rangle\langle m_{3}|_{3}\otimes|m_{7}\rangle\langle m_{7}|_{7}|G_{I}\rangle\langle G_{I}|^{\mathbf{A}_{i}\mathbf{B}_{i}\mathbf{R}}\right) = \operatorname{tr}_{\mathbf{A}_{i}\mathbf{B}_{i}}\left(|G_{I}\rangle\langle G_{I}|^{\mathbf{A}_{i}\mathbf{B}_{i}\mathbf{R}}\right) = \frac{\mathbb{I}_{1}}{2}\otimes\frac{\mathbb{I}_{6}}{2},\tag{B16}$$

from which it follows that Alice and Bob's announcements of  $\gamma_i = x_i + m_7$  and  $\delta_i = y_i + m_3$  reveal no information to the referee about  $x_i$  and  $y_i$ ; i.e.  $\sigma^{\mathbf{X}_i \mathbf{Y}_i \mathbf{R}} = \sigma^{\mathbf{X}_i \mathbf{Y}_i \mathbf{R}}_{\gamma_i, \delta_i}$ . Likewise, it is easy to see that in Stage II, the Referee's reduced state is completely mixed until all N messages are received, at which point it encodes the bit value  $\sum_{k=1}^{N} m_k$ . Now since  $f = \sum_{k=1}^{N} (m_k + \nu_k) + \sum_{i=1}^{\Re_1} b_i$ , we have that

$$p\left(\mathbf{x}_1, \cdots, \mathbf{x}_N \middle| \sum_k m_k, \{\nu_k\}_k, \{b_i\}_i\right) = p\left(\mathbf{x}_1, \cdots, \mathbf{x}_N \middle| \{\nu_k\}_k, \{b_i\}_i, f\right) = p\left(\mathbf{x}_1, \cdots, \mathbf{x}_N \middle| f\right), \tag{B17}$$

where the last equality follows from the fact that the  $\nu_k$  and  $b_i$  are independent of the  $\{\mathbf{x}_i\}_{i=1}^N$  due to the padded bits from the measurements. Hence, the Referee's knowledge of the inputs  $\{\mathbf{x}_i\}_{i=1}^N$  given the data  $(\sum_k m_k, \{\nu_k\}_k, \{b_i\}_i)$ is equivalent to his knowledge of the  $\{\mathbf{x}_i\}_{i=1}^N$  given  $f(\mathbf{x}_1, \dots, \mathbf{x}_N)$ .

## Self-testing of graph states

We can further secure the computation against an untrustworthy Source, via a self-testing procedure, which allows the parties and the Referee to validate the state distributed by the Source. If the parties indeed have the correct state, measuring the independent components of a uniformly randomly chosen stabilizer of the state will lead to a correlated outcome, hence implementing a partial test of the state's validity. By repeating the protocol and partitioning rounds between these stabilizer tests, discarded rounds of computation, and a single accepted target round of computation, the parties can upper bound the probability of receiving the incorrect state during the target round [52]. In implementing our multi-party protocol within our HoD scheme for generating the requisite states, we require the set of instructions, detailing which rounds to test, compute, and ultimately accept, be a private source of shared randomness between the parties and the Referee. This could be generated initially from a set of GHZ states distributed to the participants in the computation [58]. Without knowledge of which rounds are stabilizer tests and which are computations, the Source is prevented from modifying the state they distribute in order to fool the participants during rounds of self-testing. Conversely, the HoS scheme allows for the requisite graph states to be produced prior to the measurement-based computation protocol. Hence, the instruction set directing the participants when to self-test can be decided after the state has already been generated. In these schemes, we therefore do not require a distinct Source and Referee, at the cost of necessitating memory—in requiring the full set of photonic states be generated in advance, as well as additional rounds of self-testing [53].

## Appendix C: Constructing graph states with "emit then add"

Building graph states in either of the HoS and HoD schemes necessitates additional experimental overhead from typical deterministic quantum emitter-based schemes, in both the number of qubits required and entangling operations

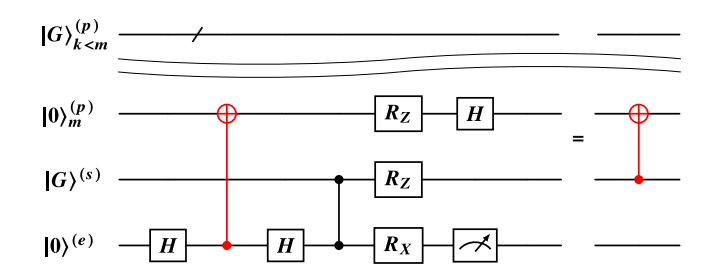


FIG. 8. A subcircuit equivalent to a  $CX_{s,p}$  gate, up to a conditional phase correction, for transferring entanglement (conditional phase information) in our proposed HoS (HoD) scheme. This example "emit then add" procedure replaces every pumping gate in typical deterministic schemes for generating arbitrary photonic graph states. Entanglement (conditional phase information) between a photon (p) and a coherently pumped emitter (e) (represented by a red  $CX_{e,p}$  gate) is exchanged to an auxiliary spin (s) via a two-qubit entangling  $CZ_{e,s}$  gate and local complementation. The emitter is measured out thereafter and reinitialized for the next iteration of the procedure. Rotations about X and Z are by  $\pi/2$  and  $-\pi/2$ , respectively, as noted in Equation (A7). The measurement of the emitter is with respect to the Z basis. All previously added photons at iterations k < m are unaffected.

between them. We demonstrate through an inductive argument that these additional resource costs scale at worst linearly. Subsequently, we present a resource-efficient set of subroutines used to produce the requisite states for our multi-party computation protocol, described in Section II. As the whole of our protocol is Clifford, we can employ the HoD scheme to produce and measure these graph states efficiently in practice, without the need for a quantum memory. We briefly discuss how phase corrections, resulting from these construction subroutines, are handled classical in this scheme. The subroutines we introduce are thereafter employed in Appendix D to estimate the fidelity to make the states used in our protocol. In what follows, a superscript (p), (s), or (e) denotes the kind of physical qubit associated with the relevant subspace on which an operator acts on, as a photon, auxiliary spin, or emitter, respectively.

### 1. Additional overhead

Let  $|G\rangle$  define an existing graph state in which there is at least a single edge between an auxiliary spin and the set of photons previously added to the graph. We label each of these photons by an emission order  $1, \dots, m-1$ . Let  $V_m$  define the additional vector space describing the emitter and the next photon, m, to be added to the graph, both of which start in  $|0\rangle$ . The set of generators which stabilizes the collective vector space  $V_G + V_m$ , consisting of the graph and subsequent emitter-photon pair, has the form

$$S_{V_G+V_m} = \langle \cdots, \cdots Z_k^{(p)} \cdots X^{(s)}, Z^{(e)}, Z_m^{(p)} \rangle, \tag{C1}$$

where  $\langle \cdots \rangle$  denotes a set of generators and the notation  $\cdots Z_k^{(p)} \cdots$  is used to keep track of an arbitrary edge between the auxiliary spin and a photon previously added to the graph at some emission step k < m. The subcircuit depicted in Figure 8 demonstrates an example of how to transfer entanglement (or conditional phase information) from the emitter-photon sub-system to  $|G\rangle$ , with a single two-qubit spin-spin entangling gate and local complementation. In implementing the example, we transform the stabilizer of the combined vector space in Equation (C1) as

$$S'_{V_G+V_m} = \langle \cdots, (-1)^{c_m} \cdots Z_k^{(p)} \cdots X_m^{(p)} X^{(s)}, (-1)^{c_m} Z_m^{(p)} Z^{(s)}, (-1)^{c_m} Z^{(e)} \rangle$$
 (C2)

where  $c_m \in \{0,1\}$  is a classical bit value conditioned on the measurement of the emitter.

The result of these operations produces the same stabilizer we would have arrived at had we instead pumped the auxiliary spin itself. With these additional operations, any graph state accessible in the deterministic scheme can be constructed in the HoS or HoD schemes. As we restrict those auxiliary spins already entangled with any previously added photons from being pumped, it follows that one additional spin, the emitter, and one two-qubit spin-spin entangling gate per photon in G are the minimum additional overhead in our proposed schemes for making arbitrary graph states. Furthermore, we can define a new vector space  $V'_G$ , containing the existing graph state and a newly entangled photon, with a dimension that increases by one with each new photon. The new space  $V'_G$  is stabilized by a unique set of generators that can be rotated back to a graph state basis of the same general form as Equation (C1), now defined by a new graph state  $|G'\rangle$ .

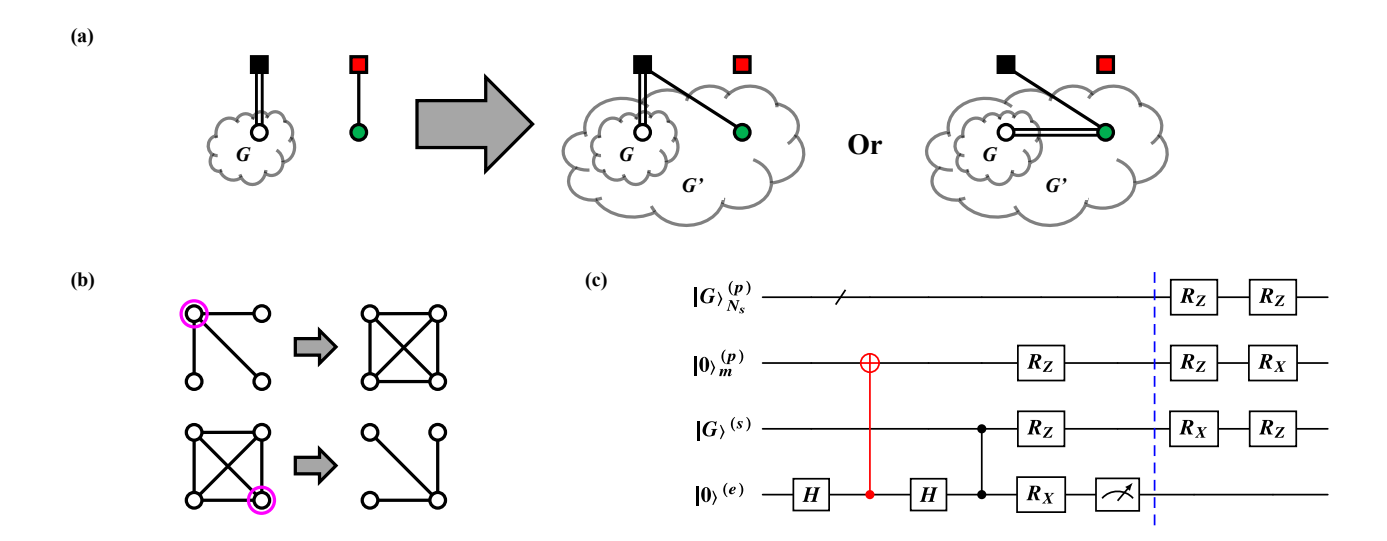


FIG. 9. Passing-subroutine for adding new photons to an existing graph, G. (a) A graph transformation of passing a new photon (green) from the emitter (red) to an auxiliary spin (black), which is connected to one or more previously added photons (white, denoted with a double edge for the multiplicity). This subroutine consists of two variations: (left) leaving all previously added photons invariant, (right) transplanting those edges to the newly added photon. (b) An example of how local complementations on a target qubit (magenta circle) can be used to add or remove edges. (c) A quantum subcircuit which implements the graph transformation. The right variation of the graph transformation above is achieved with the additional two local complementations (blue dashed line, depicting the deviation). Rotations and measurements follow the same notation as in Figure 8.

## 2. Construction subroutines

We also offer a pair of subroutines that simplifies the construction and overhead for the graph states  $|G_I\rangle$  and  $|G_{II}\rangle$ , described in Section V. Representations of the graph transformations associated with the two subroutines, along with example circuits, are depicted in Figures 9 and 10. These transformations can be performed successively with no additional operations, transforming the previous graph G built on the auxiliary spin to a new graph G' with any new photons sharing an edge to the auxiliary spin. Despite their intended application in our MPC protocol, we make no assumptions about the measurement of the photons in these subroutines, such that they can be applied generally across experimental implementations.

One "passing"-subroutine, shown in Figure 9 consists of two variations: "join" and "extend". The join-subroutine adds a new photon to an existing graph and leaves all previously existing edges invariant. The extend-subroutine transfers all edges from the auxiliary spin to the new photon. The two are achieved without or with the additional two local complementations depicted at the end of the example circuit, respectively. Both variations only act on previously added photons in the neighborhood of the auxiliary spin,  $N_s$ . Repeatedly applying the join-subroutine or extend-subroutine on a single auxiliary spin produces a star graph or linear cluster state, respectively for each variation.

We note briefly that in practice with each implementation of the passing-subroutine, the newly added photon to the graph carries a conditional phase that is a byproduct of the decoupling measurement made on the emitter, as shown in Equation (C2). This byproduct phase determines the precise basis state of the graph and may require correction for general MBQCs. In the HoD scheme, photons are measured before they are decoupled from the emitter and hence any requisite phase corrections need be commuted after each measurement. The Clifford nature of the computations employed in our MPC simplifies all of these corrections to bit flips that can be handled classically. Furthermore, correction of this phase is not always necessary as certain measurements made by the parties destroy this phase information, while other measurements allow the parties to absorb this phase information into their own pad. Conversely, conditional measurements, such as the ones made by Alice in step (4.) of Stage I of our protocol, couple these byproduct phases to the phase information input into the computation. Therefore, classical communication is required here between Alice and the Source. A simple solution is for the Source to make public the outcomes of each of these decoupling measurements.

The other "patching"-subroutine, shown in Figure 10, serves to attach two subgraphs  $G_1$  and  $G_2$  by a common edge between photons. This process requires additional two-qubit spin-spin entangling gates from the passing-subroutine.

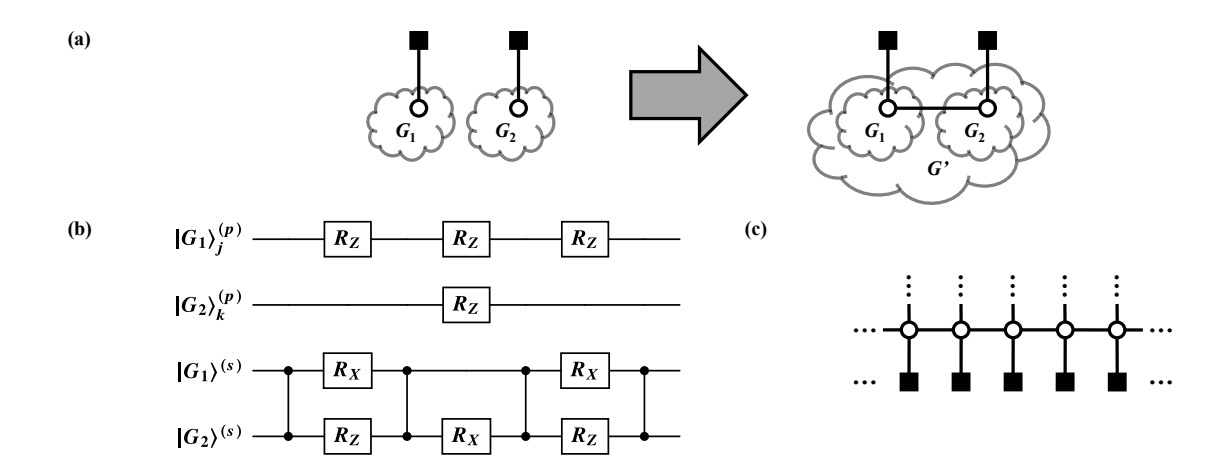


FIG. 10. Patching-subroutine for attaching two subgraphs  $G_1$  and  $G_2$  by a common edge between photons. (a) The graph transformation depicting the patching. (b) The corresponding circuit diagram. Additional two-qubit spin-spin entangling gates are required for this subroutine, over the passing-subroutine. Rotations follow the same notation as in Figure 8. (c) A 2D cluster state built on an array of auxiliary spins. Edges can be generated between photons in the layer neighboring the array of spins with this patching.

For further simplicity we only consider the case where  $G_1$  and  $G_2$  each have a single edge to all previously added photons in their respective subgraphs. Operations in this subroutine are restricted locally to only the emitter, spin, and the two photons we ultimately require to share an edge, labeled in the figure by arbitrary emission steps j, k in  $1, \dots, n_p$ . This subroutine mirrors the one employed in the production of large 2D cluster states in [5], and can be applied in either scheme we propose for the same purpose.

Application of these subroutines to the construction of the graph states discussed in Section V is straightforward. The state  $|G_I\rangle$ , consisting of  $n_p=8$  photons, labeled by an emission ordering depicted in Figure 5, can be built following the sequence of steps in Build I. This procedure requires 11 two-qubit spin-spin entangling gates in total: 8 from passing operations, and 3 from a single patching step, as we are patching between the final two photons in each subgraph and can therefore neglect the fourth spin-spin entangling gate in the subroutine. It is known that the sequential nature of photon emission events imparts an ordering on the graph state, limiting the kinds of photonic graphs accessible by construction on a single quantum emitter [59]. The private nature of the padded AND being computed in Stage I sets a nontrivial emission ordering, which, following the results of [32], requires two auxiliary spins to construct. The state  $|G_{II}\rangle$ , consisting of  $n_p=N+1$  photons for an N party computation, can be constructed entirely out of the passing-subroutine on a single auxiliary spin. This graph state can be built following Build II. Trivially, this construction requires N+1 two-qubit spin-spin entangling gates.

**Build I.**  $|G_I\rangle$ . Input: A photon emission order labeling photons  $(p_1), \dots, (p_8)$ , corresponding to the  $n_p = 8$  photons in  $|G_I\rangle$ , an emitting spin, and two auxiliary spins, labeled  $(s_1)$  and  $(s_2)$ .

- 1. Pass photon  $(p_1)$  to auxiliary spin  $(s_1)$  with join.
- 2. Pass photons  $(p_2)$  and  $(p_3)$  to  $(s_1)$ , utilizing extend for  $(p_2)$  and join for  $(p_3)$ .
- 3. Repeat the previous step for photons  $(p_4)$  and  $(p_5)$ .
- 4. Pass photon  $(p_6)$  to  $(s_1)$  with extend.
- 5. Pass photons  $(p_7)$  and  $(p_8)$  to auxiliary spin  $(s_2)$ , utilizing join for  $(p_7)$  and extend for  $(p_8)$ .
- 6. Patch subgraphs on  $(s_2)$  and  $(s_1)$ .

**Build II.**  $|G_{II}\rangle$ . Input: A photon emission order labeling photons  $(p_1), \dots, (p_N), (p_R)$ , corresponding to the  $n_p = N + 1$  photons in  $|G_{II}\rangle$ , an emitting spin, and a single auxiliary spin, labeled (s).

1. Pass photons  $(p_1), \dots, (p_N)$  to the auxiliary spin (s) with join, where photon  $(p_k)$  is routed to party k.

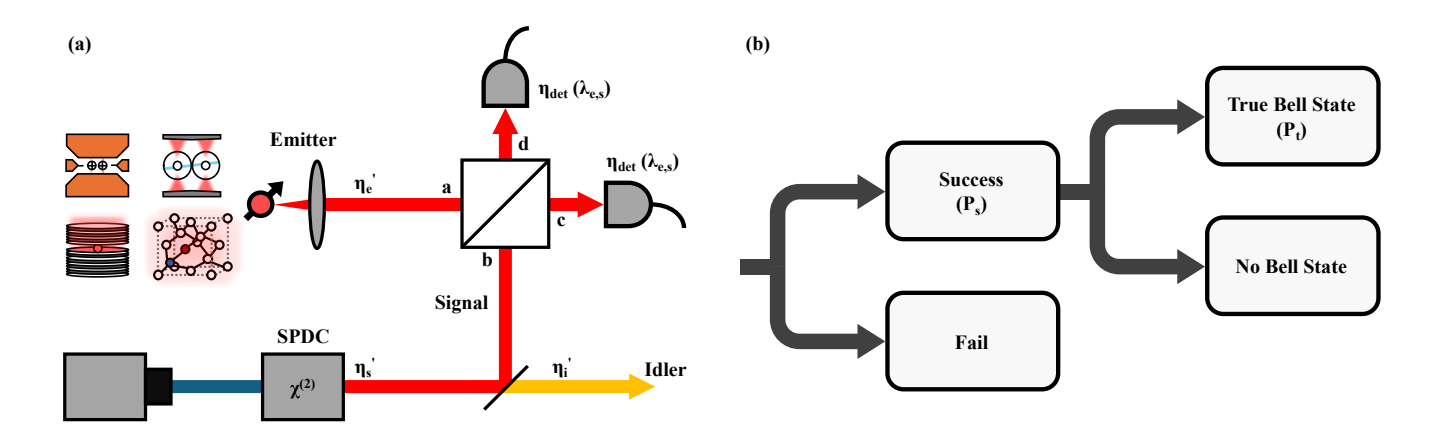


FIG. 11. Entanglement swapping in the HoS scheme. (a) Schematic of a generalized Hong-Ou-Mandel interferometer applied as a joint measurement apparatus. A photon entangled with an emitter is sent through port a of the beamsplitter, and a photon from a spontaneous parametric down conversion (SPDC) photon pair source is sent through port b. Detection of two single-photon orthonormal states  $|u\rangle$ ,  $|v\rangle$  in either output ports c or d results in entanglement between the emitter and the idler photon from the pair source. Various loss factors denoted by  $\eta$  are modeled. Additional elements for qubit rotations are not shown. (b) Probability tree showing the outcomes of a Bell state measurement attempt. The "success" probability  $P_s$  for the Bell state measurement denotes the probability of measuring a set of specific click patterns that indicate entanglement swapping.  $P_t$  denotes the probability of projecting the emitter and idler onto a Bell state per measurement attempt.

2. Pass the final photon  $(p_R)$ , belonging to the Referee, to (s) with extend.

#### Appendix D: Experimentally realizable fidelity calculations

We now consider an experimental realization of our schemes for constructing the graph states utilized in our multiparty computation. While the nature of the herald and the computation itself are device-independent, we assume here trapped ions as our quantum emitters and auxiliary spins, due to their high-fidelity benchmarks for two-qubit spin-spin entangling gates [12, 13] and reasonable collection efficiency with high-NA optics [14]. We outline our fidelity model for two schemes; the HoS scheme involving the heralding of a Bell state between an emitter and a photon for general cases involving non-destructive heralding of photons, and the HoD scheme where emitter photons are measured directly in the basis required for the measurement-based computation protocol.

# 1. Experimental apparatus

For the HoS scheme, heralding a Bell state between an emitter and photon is implemented via entanglement swapping between a photon from an emitter and a photon from a nonlinear pair source. We use spontaneous parametric down conversion (SPDC) as our pair source for the heralding. SPDC is an optical process based on a crystal with  $\chi^{(2)}$  nonlinearity whereby a photon from a pump is converted to a signal and idler photon pair of lower energy. It is often used to produce entangled photon pairs in various degrees of freedom, or as a heralded single photon source [28]. The joint measurement apparatus required for the entanglement swapping in the heralding scheme we describe here can be accomplished via a generalized Hong-Ou-Mandel interferometer [60] depicted in Figure 11(a), where the emitter photon and signal photon from the pair source are sent to a 50:50 beamsplitter. Elements from these experiments are modeled in our estimates of the fidelity to successfully produce graph states.

We briefly consider the set of states employed in heralding a Bell state in a device-independent form. The internal state of an emitter (e) is entangled with a photon  $(p_e)$  in an arbitrary basis, and an entangled photon pair is produced from the SPDC source labeled as the signal  $(p_s)$  and idler  $(p_i)$  photons. We can express both the idealized entangled

states  $|\Psi_E\rangle$  and  $|\Psi_P\rangle$ , respectively, as

$$|\Psi_E\rangle = \frac{1}{\sqrt{2}} (|0\rangle^{(e)} |1;0\rangle^{(p_e)} - |1\rangle^{(e)} |0;1\rangle^{(p_e)}),$$
 (D1)

$$|\Psi_P\rangle = \frac{1}{\sqrt{2}}(|1;0\rangle^{(p_s)}|0;1\rangle^{(p_i)} - |0;1\rangle^{(p_s)}|1;0\rangle^{(p_i)}),$$
 (D2)

where  $|0\rangle^{(e)}$  and  $|1\rangle^{(e)}$  is the computational basis for the emitter, and the notation  $|m;n\rangle$  is used to denote the photonic Fock state representation for a particular basis  $\{|u\rangle,|v\rangle\}$ , such as orthogonal polarizations, with m in  $|u\rangle$  and n in  $|v\rangle$ . The relationship between the input modes a and b and output modes b and b of the 50:50 beamsplitter can be described by the unitary transformation on the creation operators  $\hat{a}^{\dagger} = \frac{1}{\sqrt{2}}(\hat{c}^{\dagger} + \hat{d}^{\dagger})$  and  $\hat{b}^{\dagger} = \frac{1}{\sqrt{2}}(\hat{c}^{\dagger} - \hat{d}^{\dagger})$ . With the emitter photon entering port a, and the signal photon entering port b, the overall state after applying the transformation can be expressed in the form

$$\begin{split} |\Psi_{E}\rangle \, |\Psi_{P}\rangle = & \frac{(\hat{c}_{u}^{\dagger})^{2} - (\hat{d}_{u}^{\dagger})^{2}}{4} \, |vac\rangle_{c,d} \, |0\rangle^{(e)} \, |0;1\rangle^{(p_{i})} + \frac{\hat{d}_{u}^{\dagger} \hat{d}_{v}^{\dagger} - \hat{c}_{u}^{\dagger} \hat{c}_{v}^{\dagger}}{2\sqrt{2}} \, |vac\rangle_{c,d} \, |\Psi^{+}\rangle^{(e,p_{i})} \\ & + \frac{\hat{c}_{u}^{\dagger} \hat{d}_{v}^{\dagger} - \hat{c}_{v}^{\dagger} \hat{d}_{u}^{\dagger}}{2\sqrt{2}} \, |vac\rangle_{c,d} \, |\Psi^{-}\rangle^{(e,p_{i})} + \frac{(\hat{c}_{v}^{\dagger})^{2} - (\hat{d}_{v}^{\dagger})^{2}}{4} \, |vac\rangle_{c,d} \, |1\rangle^{(e)} \, |1;0\rangle^{(p_{i})} \,, \end{split} \tag{D3}$$

where

$$|\Psi^{\pm}\rangle^{(e,p_i)} = \frac{1}{\sqrt{2}}(|0\rangle^{(e)}|1;0\rangle^{(p_i)} \pm |1\rangle^{(e)}|0;1\rangle^{(p_i)}).$$
 (D4)

We are interested in projecting onto either  $|\Psi^{+}\rangle^{(e,p_i)}$  or  $|\Psi^{-}\rangle^{(e,p_i)}$  which can be realized by detecting specific click patterns on photon counting detectors at the output ports capable of resolving the orthonormal components. From Equation (D3), we can see that detecting orthonormal one-photon states in either ports c or d results in a projection onto  $|\Psi^{+}\rangle^{(e,p_i)}$  while detection in opposite ports results in  $|\Psi^{-}\rangle^{(e,p_i)}$ . The overall probability of projection onto either of the Bell states is  $\frac{1}{2}$  for each heralded measurement attempt. Upon the detection of  $|\Psi^{-}\rangle^{(e,p_i)}$ , we can perform a qubit rotation to produce the state  $|\Psi^{+}\rangle^{(e,p_i)}$  for phase consistency. We can then perform a series of one- and two-qubit gates to add a photon to a graph. Upon failure to detect the correct detection pattern, we reinitialize the emitter and photon pair and attempt the measurement again. We assume number-resolving detectors at the output ports of the beamsplitter capable of detecting photons in the basis  $\{|u\rangle,|v\rangle\}$ . For example, two polarizing beamsplitters and four detectors would be used after the output ports for photons entangled in a polarization basis.

The initial state of the emitter can be described by the state defined in Equation (D1). The output state of SPDC is a multi-mode squeezed state where the photon pair production probability is dependent on the pump amplitude. Assuming a classical pump, we take the Hamiltonian for the SPDC process to approximately be of the form [33, 61]

$$\hat{H} = e^{i\phi} \kappa \hat{K}^{\dagger} + e^{-i\phi} \kappa \hat{K}, \tag{D5}$$

where  $\hat{K}^{\dagger} = \hat{a}_{u;s}^{\dagger} \hat{a}_{v;i}^{\dagger} - \hat{a}_{v;s}^{\dagger} \hat{a}_{u;i}^{\dagger}$  represents the creation of entangled signal and idler pairs denoted s and i in the basis  $\{|u\rangle, |v\rangle\}$ . The time evolution operator  $\hat{U}(t) = \exp\left(i\hat{H}t/\hbar\right)$  yields the resulting state

$$|\Psi_{SPDC}\rangle = N \sum_{n=0}^{\infty} \tanh^n r \sum_{m=0}^{n} (-1)^m |n-m;m\rangle^{(p_s)} |m;n-m\rangle^{(p_i)},$$
 (D6)

where  $r = \kappa t/\hbar$  is the interaction parameter that is dependent on the pump field amplitude, t is the interaction time of the pump through the crystal, and N is the normalization constant with  $N = 1 - \tanh^2 r$ . By tuning the interaction parameter r, we can change the probability of producing a single pair (n = 1 in Equation (D6)) leading to Equation (D2)) to optimize the fidelity of the HoS scheme. Note that increasing the pump power also increases the relative contribution of the higher order terms (n > 1), which increases the probability of detecting multiple photon pairs.

The above is applicable for polarization-entangled photon pairs directly produced in type-II SPDC described in refs. [33, 61]; the output state and choice of degree-of-freedom for entanglement will of course be dependent on the specific properties of the photon pair source and pump. However, we note that we are assuming the pump can be treated as a classical, single-mode source, and we use a simplified Hamiltonian and output state for the photon pairs entangled in  $\{|u\rangle, |v\rangle\}$ . Moreover, factors such as the multi-modal nature of the pump, phase differences or instabilities between the orthonormal components in the optical path, or distinguishability between the photons from the emitter and the SPDC source can degrade the fidelity of the scheme.

#### 2. Sources of infidelity

Several experimentally relevant sources of infidelity are considered in our model. Photonic loss and detector dark counts can induce false heralding events, leading to a failure to resolve a true Bell state and subsequent addition of a photon to the graph. Decoherence across the emitter and any auxiliary spins utilized in building the graph will produce errors on any computation done on the graph state. The fidelity of each two-qubit spin-spin entangling gate performed in the construction is considered as well. We can also consider the fidelity of the initial entanglement between the emitter and its photon, as well as the entanglement of the photon pair, used in the entanglement swapping procedure.

#### a. Photonic loss

We use the standard approach to modeling photonic losses, which is to introduce a fictitious beamsplitter with transmittance  $\eta$  and reflectance  $1-\eta$  on the lossy channel. This is equivalent to applying the transformation on the creation operator  $\hat{a}^{\dagger} = \sqrt{\eta} \hat{a}_T^{\dagger} + \sqrt{1-\eta} \hat{a}_R^{\dagger}$  [62] where T and R denote the transmitted and reflected paths, respectively. The Fock state  $|n\rangle$  serving as the input transforms as  $|n\rangle \to \sum_{k=0}^{n} \sqrt{\binom{n}{k} \eta^{n-k} (1-\eta)^k} |n-k\rangle_T |k\rangle_R$  and the reflected path is traced out. We assume, for simplicity, that  $\eta$  is independent of the photonic degrees of freedom for each loss channel modeled. Applying this to an emitter with an initial state given by Equation (D1) and performing the partial trace over the reflected path, the resulting density matrix  $\hat{\rho}_E$  for the emitter-photon pair incorporating losses is

$$\hat{\rho}_{E} = \frac{1}{2} (1 - \eta_{e}) |0\rangle\langle 0|^{(e)} \otimes |vac\rangle\langle vac|^{(p_{e})} + \frac{1}{2} (1 - \eta_{e}) |1\rangle\langle 1|^{(e)} \otimes |vac\rangle\langle vac|^{(p_{e})}$$

$$+ \frac{1}{2} \eta_{e} |0\rangle\langle 0|^{(e)} \otimes |1; 0\rangle\langle 1; 0|^{(p_{e})} + \frac{1}{2} \eta_{e} |1\rangle\langle 1|^{(e)} \otimes |0; 1\rangle\langle 0; 1|^{(p_{e})}$$

$$- \frac{1}{2} \eta_{e} |0\rangle\langle 1|^{(e)} \otimes |1; 0\rangle\langle 0; 1|^{(p_{e})} - \frac{1}{2} \eta_{e} |1\rangle\langle 0|^{(e)} \otimes |0; 1\rangle\langle 1; 0|^{(p_{e})}.$$
(D7)

Similarly, the density matrix for the SPDC source  $\hat{\rho}_{SPDC}$  becomes

$$\hat{\rho}_{SPDC} = \sum_{n,n^*=0}^{\infty} \sum_{m=0}^{n} \sum_{m^*=0}^{n^*} \sum_{k_s,k_i'=0}^{\min\{n-m,n^*-m^*\}} \sum_{k_s',k_i=0}^{\min\{m,m^*\}} c_{n,m,k_s,k_s',k_i,k_i'} c_{n^*,m^*,k_s,k_s',k_i,k_i'}^*$$

$$|n-m-k_s;m-k_s'\rangle \langle n^*-m^*-k_s;m^*-k_s'|^{(p_s)}$$

$$\otimes |m-k_i;n-m-k_i'\rangle \langle m^*-k_i;n^*-m^*-k_i'|^{(p_i)},$$
(D8)

where

$$c_{n,m,k_s,k'_s,k_i,k'_i} = (1-\xi)(\sqrt{\xi})^n (-1)^m \sqrt{\binom{n-m}{k_s}\binom{m}{k'_s}\binom{m}{k_i}\binom{n-m}{k'_i}\eta_s^{n-k_s-k'_s}(1-\eta_s)^{k_s+k'_s}\eta_i^{n-k_i-k'_i}(1-\eta_i)^{k_i+k'_i}},$$
(D9)

and we have used  $\xi = \tanh^2 r$ . Here, we have made the additional substitutions  $\eta_e = \eta_e' \eta_{det}(\lambda_e)$  and  $\eta_s = \eta_s' \eta_{det}(\lambda_s)$ , where  $\eta_e$  and  $\eta_s$  are the combined collection and photodetection efficiencies for the emitter and signal photons, respectively, in the interferometry setup.  $\eta'$  accounts for the collection efficiency of the optical path as shown in Figure 11(a), and  $\eta_{det}(\lambda)$  is the photodetection efficiency which may be wavelength dependent (in the joint measurement, we require  $\lambda_e = \lambda_s$ ).  $\eta_i = \eta_i'$  is the collection efficiency of the idler for the SPDC setup, neglecting user-specific losses such as transmission losses through an optical fiber network and imperfect detection from the user. Since we are interested in retrieving the photon from the emitter and a single pair from the SPDC source for entanglement swapping, under the loss model the resulting probabilities for  $|\Psi_E\rangle$  and  $|\Psi_P\rangle$  as defined in Equation (D1) and Equation (D2) are

$$\langle \Psi_E | \hat{\rho}_E | \Psi_E \rangle = \eta_e, \tag{D10}$$

$$\langle \Psi_P | \hat{\rho}_{SPDC} | \Psi_P \rangle = \frac{\eta_s \eta_i \xi(\bar{\eta}_s \bar{\eta}_i \xi + 2) (1 - \xi)^2}{(1 - \bar{\eta}_s \bar{\eta}_i \xi)^4},$$
 (D11)

where  $\bar{\eta}_e = 1 - \eta_e$ ,  $\bar{\eta}_s = 1 - \eta_s$ , and  $\bar{\eta}_i = 1 - \eta_i$ .

#### b. Photodetector metrics

In this work, we provide practical estimates of the fidelity achievable using photon number-resolving detectors for entanglement swapping. We assume each detector in the setup has some efficiency  $\eta_{det}$  and also model dark counts which arise due to inherent electronic noise in a detector. Each dark count event is assumed to be independent and generated at a constant rate  $R_d$  cps, and typically dark count rates can be low ( $< 10^{-2}$  cps) for single-photon detectors such as Transition Edge Sensors [63]. Furthermore, we assume the exposure time of the detectors,  $t_{\rm exp}$  is much longer than the time scale over which dark counts emerge. The probability for  $n_d$  dark counts on a detector during each measurement cycle can then be approximated by a Poisson distribution [64]

$$P_d(n_d) = e^{-R_d t_{\text{exp}}} \frac{(R_d t_{\text{exp}})^{n_d}}{n_d!}.$$
 (D12)

The joint measurement in the heralding involves the use of detectors in output ports c and d in Figure 11. Therefore, we need to consider the effect of four detection outcomes for the herald – two detectors each with two orthonormal results, and the probability of dark counts for each. We assume identical dark count distributions for the detectors used in the herald.

## c. Entanglement swapping and heralded success probability

A successful herald occurs at a probability which we define as  $P_s$ . For the HoD scheme,  $P_s = \eta_e$  as we perform additional single and two-qubit operations on a graph only when the photon from the emitter is successfully measured. In the HoS scheme,  $P_s$  is the probability of detecting the set of detector click patterns requisite for the entanglement swap.

An extra source of infidelity for the heralded Bell state measurement occurs from the joint measurement itself. We define  $P_t$  as the overall probability of projecting the idler photon and emitter onto a Bell state for each joint measurement attempt. The probabilities are indicated in Figure 11(b). This will be a function of the detection efficiencies of the photons as well as the probability of zero dark count events detected. From Equation (D10), Equation (D11), and Equation (D12),  $P_t$  is given by

$$P_{t}(\eta_{e}, \eta_{s}, \eta_{i}, \xi) = \frac{1}{2} \langle \Psi_{E} | \hat{\rho}_{E} | \Psi_{E} \rangle \langle \Psi_{P} | \hat{\rho}_{SPDC} | \Psi_{P} \rangle P_{d}^{4}(0)$$

$$= \frac{1}{2} \frac{\eta_{e} \eta_{s} \eta_{i} \xi(\bar{\eta}_{s} \bar{\eta}_{i} \xi + 2)}{(1 - \bar{\eta}_{s} \bar{\eta}_{i} \xi)^{4}} (1 - \xi)^{2} P_{d}^{4}(0). \tag{D13}$$

The heralded success probability  $P_s$  for the joint measurement is conditioned on a detection pattern representing the orthonormality of the photon states after the beamsplitter. This is a source of infidelity as the joint detection of states such as  $|0;0\rangle^{(p_e)}|1;1\rangle^{(p_s)}$ , representing two signal photons that are orthonormal to each other from the photon pair source and no photons from the emitter, possible due to detection or collection losses, would not result in entanglement swapping. We can identify the set of states that would result in a "success":

$$S = \{ |1;0\rangle^{(p_e)} |0;1\rangle^{(p_s)}, |0;1\rangle^{(p_e)} |1;0\rangle^{(p_s)}, |0;0\rangle^{(p_e)} |1;1\rangle^{(p_s)} \}$$
(D14)

For each state in the set S, dark counts can lead to a false detection of the state. For example, the state  $|1;0\rangle^{(p_e)}|0;1\rangle^{(p_s)}$  with zero dark counts is indistinguishable from the state  $|1;0\rangle^{(p_e)}|0;0\rangle^{(p_s)}$  with one dark count falsely attributed to the measurement of a signal photon in the state  $|0;1\rangle^{(p_s)}$ . The former has an additional associated dark count probability of  $P_d^4(0)$  and the latter  $P_d(1)P_d^3(0)$ . Thus, we can compute  $P_s$  by considering the probability of measuring all states in S and all dark count combinations and photon number states that reconstruct each element of S. By taking the partial trace of the emitter and idler photon from Equation (D7) and Equation (D8), and considering the probabilities mentioned in the overall set of joint measurement outcomes, we arrive at the probability  $P_s$  for the joint measurement,

$$P_{s}(\eta_{e}, \eta_{s}, \xi) = \frac{3\bar{\eta}_{e}}{(1 - \bar{\eta}_{s}\xi)^{2}} (1 - \xi)^{2} P_{d}^{2}(1) P_{d}^{2}(0)$$

$$+ \left[ \frac{\eta_{e}}{(1 - \bar{\eta}_{s}\xi)^{2}} + \frac{4\bar{\eta}_{e}\eta_{s}\xi}{(1 - \bar{\eta}_{s}\xi)^{3}} \right] (1 - \xi)^{2} P_{d}(1) P_{d}^{3}(0)$$

$$+ \left[ \frac{\eta_{e}\eta_{s}\xi}{(1 - \bar{\eta}_{s}\xi)^{3}} + \frac{\bar{\eta}_{e}\eta_{s}^{2}\xi^{2}}{(1 - \bar{\eta}_{s}\xi)^{4}} \right] (1 - \xi)^{2} P_{d}^{4}(0). \tag{D15}$$

In this paper, we consider the case where heralding is repeated until a "success" is flagged for each idler photon added to the graph. Thus, the fidelity of the entanglement swapping procedure is  $F_{\text{swap}} = P_t/P_s$ .

#### d. Decoherence

The emitter used to generate photons, as well as any auxiliary spins entangled with an existing graph, will dephase across the duration until they are measured and projected back onto a known state. For an emitter or auxiliary spin represented by a density matrix  $\hat{\rho}$ , we model the dephasing process via the map

$$\hat{\rho} \to \mathcal{D}(\hat{\rho}; t, \tau) = \frac{1}{2} (1 + e^{-t/\tau}) \hat{\rho} + \frac{1}{2} (1 - e^{-t/\tau}) Z \hat{\rho} Z, \tag{D16}$$

where  $\tau$  is the coherence time of the emitter or auxiliary spin and t is a timescale for the dephasing process. Clearly this process leaves the state invariant with probability  $\frac{1}{2}(1+e^{-t/\tau})$ , or conjugates it by Z with probability  $\frac{1}{2}(1-e^{-t/\tau})$ . It is straightforward to verify that this map describes a Markovian process such that

$$\mathcal{D}(\hat{\rho}; t_1 + t_2, \tau) = \mathcal{D}(\hat{\rho}; t_2, \tau) \circ \mathcal{D}(\hat{\rho}; t_1, \tau). \tag{D17}$$

We assume that each attempted herald happens on a short, regular timescale  $t_{\rm rep}=R_{\rm rep}^{-1}$ , which is simply the inverse repetition rate of the experiment. Furthermore, we assume each qubit gate operation time is near-instantaneous compared to  $t_{\rm rep}$ , so that the dephasing takes place during the attempted herald only. As the emitter is measured out and reinitialized with each cycle of the experiment, it is evident that it will only dephase for at most  $t_{\rm rep}$ . This implies that for each photon added to the graph, the contribution to the graph state fidelity from the decoherence of the emitter is  $\frac{1}{2}(1 + e^{-t_{\rm rep}/\tau_e})$ , such that

$$F_D^{(e)}(n_p) = \left(\frac{1}{2}\left(1 + e^{-t_{\text{rep}}/\tau_e}\right)\right)^{n_p},$$
 (D18)

is the total contribution towards building an  $n_p$ -photon graph state, and  $\tau_e$  is the coherence time for the emitter.

We now model the contribution to the final state fidelity from any auxiliary spins in the system, which dephase for the entirety of their presence in the graph. Consider a mixed state density operator  $\hat{\rho}_n = \sum_{\lambda} p_{\lambda} |\Phi_{\lambda}\rangle\langle\Phi_{\lambda}|$ , described by a convex combination of n-qubit pure stabilizer states  $|\Phi_{\lambda}\rangle$ , where  $p_{\lambda}$  are the corresponding classical probabilities. This could represent the mixture of states one expects for an existing graph state built on a set of auxiliary spins, when under the action of its environment—including the prior action of the dephasing map itself. The system is initially stabilized by a set of generators  $S_{|\Phi_{\lambda}\rangle} = \langle g_{1,\lambda}, g_{2,\lambda}, \cdots, g_{n,\lambda} \rangle$ . Under the dephasing map the state evolves as

$$\mathcal{D}^{(s)}(\hat{\rho}_n; t, \tau_s) = \frac{1}{2} (1 + e^{-t/\tau_s}) \sum_{\lambda} p_{\lambda} |\Phi_{\lambda}\rangle\langle\Phi_{\lambda}| + \frac{1}{2} (1 - e^{-t/\tau_s}) \sum_{\lambda} p_{\lambda} Z^{(s)} |\Phi_{\lambda}\rangle\langle\Phi_{\lambda}| Z^{(s)}, \tag{D19}$$

which is once again a convex combination of stabilizer states with generators

$$S_{|\Phi_{\lambda}\rangle} = \langle g_{1,\lambda}, g_{2,\lambda}, \cdots, g_{n,\lambda}\rangle,$$

$$S_{Z^{(s)}|\Phi_{\lambda}\rangle} = \langle Z^{(s)}g_{1,\lambda}Z^{(s)}, Z^{(s)}g_{2,\lambda}Z^{(s)}, \cdots, Z^{(s)}g_{n,\lambda}Z^{(s)}\rangle.$$
(D20)

 $\tau_s$  is the coherence time of the auxiliary spins in the system, which we treat as identical. Since we are interested in graph states,  $\hat{\rho}_{G=(V,E)} = |G\rangle\langle G|$ , whose stabilizers are generated by the operators  $\{K_a\}_{a\in V}$  defined in Equation (A3), the dephasing map only acts on the generators proportional to  $X^{(s)}$ , for any auxiliary spin (s) in the system. Hence, a graph state consisting of  $n_p$  photons and  $n_s$  auxiliary spins would evolve under the dephasing map as the mixture

$$\mathcal{D}^{(s)}(\hat{\rho}_G; t, \tau_s) = \sum_{\mathbf{b} \in \mathbb{Z}_2^{n_s}} p(\mathbf{b}) |G_{\mathbf{b}}\rangle \langle G_{\mathbf{b}}|, \qquad (D21)$$

where  $\mathbf{b} = (b_1, b_2, \cdots, b_{n_s}) \in \mathbb{Z}_2^{n_s}$  and

$$p(\mathbf{b}) = \frac{1}{2^{n_s}} \prod_{i=1}^{n_s} (1 + (-1)^{b_i} e^{-t/\tau_s}).$$
 (D22)

This mixture is stabilized by the set of generators,

$$S_{|G_{\mathbf{b}}\rangle} = \langle K_1^{(p)}, \cdots, K_{n_p}^{(p)}, (-1)^{b_1} K_1^{(s)}, \cdots, (-1)^{b_{n_s}} K_{n_s}^{(s)} \rangle.$$
 (D23)

The size of the system's stabilizer grows by one with each new photon m added to the graph. For the passing-subroutines we employ in Appendix C 2, we apply this rule, however in choosing either variation of the subroutine we choose whether to rotate the auxiliary spin out of the basis of the dephasing map, and consequentially project the system onto a new mixed state as described above. That is for the  $m^{\text{th}}$  photon, we generate a new subgroup of the stabilizer as either

$$S_{|G\rangle,\text{join}-m} = \langle (-1)^{b_k} \cdots Z_k^{(p)} \cdots Z_m^{(p)} X^{(s)}, X_m^{(p)} Z^{(s)} \rangle, \tag{D24a}$$

$$S_{|G\rangle, \text{extend}-m} = \langle (-1)^{b_k} \cdots Z_k^{(p)} \cdots X_m^{(p)} Z^{(s)}, Z_m^{(p)} X^{(s)} \rangle.$$
 (D24b)

Here, the bit conditioning phase  $b_k$  is applied to the generator  $K^{(s)}$  during the creation of the  $k^{\text{th}}$  photon, with k < m. If we allow the system to continue dephasing, these subgroups evolve, distinctly, as

$$S_{|G_{\mathbf{b}}\rangle, \text{join}-m} = \langle (-1)^{b_k + b_m} \cdots Z_k^{(p)} \cdots Z_m^{(p)} X^{(s)}, X_m^{(p)} Z^{(s)} \rangle,$$
 (D25a)

$$S_{|G_{\mathbf{b}}\rangle, \text{extend}-m} = \langle (-1)^{b_k} \cdots Z_k^{(p)} \cdots X_m^{(p)} Z^{(s)}, (-1)^{b_m} Z_m^{(p)} X^{(s)} \rangle. \tag{D25b}$$

We see that in the case of executing the extend-subroutine on  $m^{\text{th}}$  photon, the number of states in the mixture doubles, whereas in the case of the join-subroutine, the symmetry between states where either  $b_k = b_m$  or  $b_k \neq b_m$  leads to an effective mixture the same size as it was prior to the  $m^{\text{th}}$  photon's addition. Furthermore, we can express the probability for each state in the mixture in terms of  $b_k$  and  $b_m$  as

$$P(b_k, b_m) = \frac{1}{4} \left( 1 + (-1)^{b_k} e^{-t_k/\tau_s} \right) \left( 1 + (-1)^{b_m} e^{-t_m/\tau_s} \right).$$
 (D26)

where we have defined  $t_k$  and  $t_m$  as arbitrary times from the probabilistic nature of the herald. For the join-subroutine, the graph state remains unchanged when  $b_k, b_m = 0$  or  $b_k, b_m = 1$ , whereas, for the extend-subroutine, the graph state remains unchanged only when  $b_k, b_m = 0$ . Hence, the fidelity under the dephasing model scales as  $\frac{1}{2}(1 + e^{-(t_k + t_m)/\tau_s})$  for the join-subroutine and  $\frac{1}{4}(1 + e^{-t_k/\tau_s})(1 + e^{-t_m/\tau_s})$  for the extend-subroutine for iterations k and m. This is a subtle distinction that arises from the Markovian nature of the dephasing map when implementing the join-subroutine. It implies the final state fidelity when constructing graph states on a set of auxiliary spins will in general depend on the sequence describing how each photon is passed into the system. In contrast, we assume  $t_{\rm rep} \ll \tau_s$  in our estimates, such that this distinction is not necessary, as  $\frac{1}{4}(1 + e^{-t_k/\tau_s})(1 + e^{-t_m/\tau_s}) \approx \frac{1}{2}(1 + e^{-(t_k + t_m)/\tau_s})$ . We provide estimates where  $t_{\rm rep}/\tau_s$  is of order  $10^{-7} - 10^{-9}$  [10, 31]. It is nonetheless important to discuss, when considering auxiliary spins with shorter coherence times or constructing exceedingly large graph states, where the time to build the graph is of order the coherence time.

Lastly, we account for the probabilistic nature of the herald. Building graph states using either scheme we propose can be viewed as a Bernoulli trial with success probability  $P_s$  occurring at regular intervals  $t_{\rm rep}$ . The cumulative probability that m trials yields r successes is given by the distribution

$$h(m, r, P_s) = {\binom{m-1}{r-1}} P_s^r (1 - P_s)^{m-r},$$
(D27)

where  $m = r, r + 1, r + 2, \cdots$ . For any auxiliary spins in the graph, any failure to herald adds an additional  $t_{\text{rep}}$  to the dephasing time. Therefore, we model the mean contribution to the state fidelity for an auxiliary spin with r photons passed to it under either passing-subroutine as

$$\langle F_D^{(s)}(r, P_s) \rangle = \sum_{m=r}^{\infty} h(m, r, P_s) \left( \frac{1}{2} \left( 1 + e^{-mt_{\text{rep}}/\tau_s} \right) \right)$$

$$= \frac{1}{2} \left( 1 + \left( \frac{P_s}{P_s + e^{t_{\text{rep}}/\tau_s} - 1} \right)^r \right)$$

$$\approx \frac{1}{2} \left( 1 + e^{-rt_{\text{rep}}/P_s\tau_s} \right), \tag{D28}$$

where  $\langle \cdots \rangle$  here denotes a classical expectation value, and  $t_{\rm rep}/P_s$  is the average time for a successful herald. Note in the HoD scheme,  $P_s = \eta_e$ , whereas in the HoS scheme it is of the form in Equation (D15). For an  $n_p$ -photon graph state, we take r up to the number of photons that a given auxiliary spin remains a part of the graph. Here, we consider the same coherence times for the emitter and auxiliary spins,  $\tau_e = \tau_s = \tau$ . Given state-of-art of trapped ion experiments [10], we take the dephasing timescale to be  $t_{\rm rep}/\tau = 10^{-9}$  in our best estimates.

Single-qubit gates applied to photons, the emitter and any auxiliary spins are assumed to be perfect in our model. For all two-qubit spin-spin entangling gates, we assume a fidelity  $F_{CZ} = 0.999$  in our best estimates, in line with benchmarks from state-of-the-art trapped ion experiments [12, 13]. We assume the time to implement any single-qubit or two-qubit gate,  $t_{\text{gate}} \ll t_{\text{rep}}$ , and can therefore be treated as instantaneous.

## f. Initial entanglement fidelity

In practice, there will be a non-unit fidelity on initializing the emitter onto the state described in Equation (D1) as well as Equation (D2) for the pair source. The additional contribution to the overall fidelity using our schemes, as compared to schemes where an emitter is directly used to generate graphs, is the entanglement fidelity of the nonlinear photon pair source in our HoS scheme. For example, the main contribution to the degradation of polarization-based entanglement fidelity for a single photon pair in SPDC comes from the spatial-temporal profile of the pump [65] and its interaction with the specific nonlinear medium, in which different spatial and spectral or temporal components impart different relative phases to the entangled pair described by Equation (D2). The fidelity can be optimized by using compensating crystals or filtering techniques; however, the latter also lowers the collection efficiency. Nevertheless, some of the best estimated fidelities for polarization-entangled SPDC sources range from  $\sim 97\%$  to  $\sim 99.7\%$  for various free-space and fiber-based setups [66–68]. In terms of overall fidelity estimations, we can introduce additional scaling terms similar to the gate fidelity described above. We denote the initial entanglement fidelities for the emitter photon and photon-photon pair as  $F_e$  and  $F_p$ , respectively. We focus primarily on the fidelity from the SPDC source to highlight the additional infidelity from our scheme.

#### 3. Pair generation rate optimization

Given the infidelity from false heralds, defined in Equations D13 and D15, there exists a trade-off between the rate and fidelity at which large graph states can be generated in the HoS scheme, as set by the dimensionless parameter  $\xi$ , controlling the pair generation rate of the SPDC source. Decreasing  $\xi$  improves the probability of heralding a true Bell state, at the cost of longer average times between successful heralds. Conversely, the effects of decoherence on any auxiliary spins in the system, through Equation (D28), reduces the fidelity of the graph state, as the overall construction time increases. Hence, there is an optimum rate at which HoS can run, controlled by  $\xi$  and parameterized by the relevant total collection and detection efficiencies  $\{\eta_e, \eta_s, \eta_i\}$ , dark count rate,  $R_d$ , dephasing timescale,  $t_{\rm rep}/\tau$ , number of auxiliary spins,  $n_s$ , and total number of photons,  $n_p$ , required by the graph. Given a fixed set of parameters, this is a straightforward scalar maximization problem that can be accomplished numerically. If necessary, one can optimize within some  $\epsilon$  of the optimum in order to achieve a speed-up in the rate.

### 4. Example applications

We briefly demonstrate how the sources of infidelity, presented in Appendix D 2, are combined to produce the fidelity estimates discussed in Sections IV and V. We note from the above that this fidelity is a mean estimate, optimized over  $\xi$ . For the estimates discussed in our work, we assume a negligible dark count rate, and let  $\eta_s = \eta_i = 1$ . In practice the signal photon collection efficiency can be near unity [31], and only makes a minor impact on the rate and fidelity that does not affect the overall scaling of either function, relative to the other relevant parameters. We carry out the optimization numerically, and determine  $\xi$  which achieves the optimum fidelity, when considering estimates in our HoS scheme.

# a. GHZ states and cluster states

In Section IV, we present the mean final state fidelity to generate arbitrary graph states, requiring a single auxiliary spin in either of our schemes, such as the  $n_p$ -photon star graph, which is local-unitary equivalent to a GHZ state, or a 1D cluster state. For these graph states we optimize a function of the form

$$F_{n_s=1}(\xi; n_p, \eta_e) = (F_{\text{ent}} F_{\text{swap}}(\xi; \eta_e))^{n_p} F_D^{(e)}(n_p) \langle F_D^{(s)}(n_p, P_s(\eta_e, \xi)) \rangle.$$
(D29)

Here, we have defined  $F_{\rm ent} = F_{CZ} F_p$  to combine the spin-spin entangling gate and photon pair entanglement fidelities, respectively. In Figure 4, we compare the effects of false heralds and decoherence against the limits imposed by imperfect spin-spin gate and initial SPDC photon pair entanglement fidelities, and hence set  $F_{\rm ent} = 1$  when computing estimates in the false herald and decoherence limited regimes. In the decoherence limited regime we additionally set  $F_{\rm swap} = 1$  and subsequently do not require optimization. Computing the fidelity to make these states in our schemes with perfect spin-spin entangling gates and initial photon pair entanglement assumes that additional error-correction or purification is employed.

#### b. Multi-party computation

For the MPC introduced in Section V, fidelity estimates for the generation of  $|G_I\rangle$  and  $|G_{II}\rangle$  are required to estimate the total bit error probability in Stage I and II, respectively. We assume graph states constructed in the HoD scheme discussed in Section III, where the computation of f happens in parallel with the construction of each state, and no pair source or photonic memory is required. In this scheme we take  $P_s = \eta_e = 0.4$ , from trapped ion experiments utilizing parabolic reflectors [17]. Additionally, we assume a dephasing timescale  $t_{\rm rep}/\tau = 10^{-9}$ , following the best estimates for trapped ions [10]. The production of arbitrarily large graph states using our scheme is predominately limited by the spin-spin entangling gate fidelity and photon pair entanglement fidelity,  $F_{CZ}$  and  $F_p$ , respectively. However, for a fixed number of parties N, the size of the required graph states for our protocol is also fixed. For each iteration of Stage I, the Source is required to generate a copy of the 8-qubit graph state,  $|G_I\rangle$ , depicted in Figure 5. From Equation (D18) and Equation (D28), the mean fidelity to produce each copy of the state is

$$F_{G_I} = F_{\text{ent}}^8 F_{CZ}^3 F_D^{(e)}(8) \langle F_D^{(s_1)}(8, \eta_e) \rangle \langle F_D^{(s_2)}(2, \eta_e) \rangle, \tag{D30}$$

where we have defined again  $F_{\rm ent}=F_{CZ}F_p$ . We note additional spin-spin entangling gates are required to make this graph state, as compared to Equation (D29). In Stage II, the source distributes a single copy of the N+1-qubit graph state,  $|G_{II}\rangle$ , depicted in Figure 6, where N is number of parties involved in the computation. The mean fidelity to produce this state is

$$F_{G_{II}}(N) = F_{\text{ent}}^{N+1} F_D^{(e)}(N+1) \langle F_D^{(s)}(N+1, \eta_e) \rangle, \tag{D31}$$

which is equivalent to fidelity in Equation (D29), upon setting  $n_p = N + 1$ .

- R. Raussendorf and H. J. Briegel, Phys. Rev. Lett. 86, 5188 (2001).
- [2] D. E. Browne and T. Rudolph, Phys. Rev. Lett. 95, 010501 (2005).
- [3] N. H. Lindner and T. Rudolph, Phys. Rev. Lett. 103, 113602 (2009).
- [4] S. E. Economou, N. Lindner, and T. Rudolph, Phys. Rev. Lett. 105, 093601 (2010).
- [5] A. Russo, E. Barnes, and S. E. Economou, New Journal of Physics 21, 055002 (2019).
- [6] P. Hilaire, L. Vidro, H. S. Eisenberg, and S. E. Economou, Quantum 7, 992 (2023).
- [7] Y. Zhan and S. Sun, Physical Review Letters 125, 223601 (2020).
- [8] D. Cogan, Z.-E. Su, O. Kenneth, and D. Gershoni, Nature Photonics 17, 324–329 (2023).
- [9] D. Bluvstein, H. Levine, G. Semeghini, T. T. Wang, S. Ebadi, M. Kalinowski, A. Keesling, N. Maskara, H. Pichler, M. Greiner, V. Vuletić, and M. D. Lukin, Nature 604, 451–456 (2022).
- [10] P. Wang, C.-Y. Luan, M. Qiao, M. Um, J. Zhang, Y. Wang, X. Yuan, M. Gu, J. Zhang, and K. Kim, Nature

- communications **12**, 1 (2021).
- [11] S. J. Evered, D. Bluvstein, M. Kalinowski, S. Ebadi, T. Manovitz, H. Zhou, S. H. Li, A. A. Geim, T. T. Wang, N. Maskara, H. Levine, G. Semeghini, M. Greiner, V. Vuletić, and M. D. Lukin, Nature 622, 268–272 (2023).
- [12] R. Srinivas, S. C. Burd, H. M. Knaack, R. T. Sutherland, A. Kwiatkowski, S. Glancy, E. Knill, D. J. Wineland, D. Leibfried, A. C. Wilson, D. T. C. Allcock, and D. H. Slichter, Nature 597, 209–213 (2021).
- [13] C. R. Clark, H. N. Tinkey, B. C. Sawyer, A. M. Meier, K. A. Burkhardt, C. M. Seck, C. M. Shappert, N. D. Guise, C. E. Volin, S. D. Fallek, H. T. Hayden, W. G. Rellergert, and K. R. Brown, Physical Review Letters 127, 10.1103/physrevlett.127.130505 (2021).
- [14] G. Shu, C.-K. Chou, N. Kurz, M. R. Dietrich, and B. B. Blinov, J. Opt. Soc. Am. B 28, 2865 (2011).
- [15] D. Hucul, I. V. Inlek, G. Vittorini, C. Crocker, S. Debnath, S. M. Clark, and C. Monroe, Nature Physics 11, 37 (2015).
- [16] C.-K. Chou, C. Auchter, J. Lilieholm, K. Smith, and B. Blinov, Review of Scientific Instruments 88 (2017).

- [17] R. Maiwald, A. Golla, M. Fischer, M. Bader, S. Heugel, B. Chalopin, M. Sondermann, and G. Leuchs, Physical Review A 86, 043431 (2012).
- [18] A. Kinos, D. Hunger, R. Kolesov, K. Mølmer, H. de Riedmatten, P. Goldner, A. Tallaire, L. Morvan, P. Berger, S. Welinski, et al., arXiv preprint arXiv:2103.15743 (2021).
- [19] R. Yanagimoto, R. Nehra, R. Hamerly, E. Ng, A. Marandi, and H. Mabuchi, PRX Quantum 4, 010333 (2023).
- [20] S. E. Economou, L. J. Sham, Y. Wu, and D. G. Steel, Phys. Rev. B 74, 205415 (2006).
- [21] M. Gimeno-Segovia, T. Rudolph, and S. E. Economou, Phys. Rev. Lett. 123, 070501 (2019).
- [22] D. Rieländer, A. Lenhard, M. Mazzera, and H. De Riedmatten, New Journal of Physics 18, 123013 (2016).
- [23] J. P. Covey, H. Weinfurter, and H. Bernien, npj Quantum Information 9, 10.1038/s41534-023-00759-9 (2023).
- [24] T. Ward and M. Keller, New Journal of Physics 24, 123028 (2022).
- [25] V. Krutyanskiy, M. Galli, V. Krcmarsky, S. Baier, D. A. Fioretto, Y. Pu, A. Mazloom, P. Sekatski, M. Canteri, M. Teller, J. Schupp, J. Bate, M. Meraner, N. Sangouard, B. P. Lanyon, and T. E. Northup, Phys. Rev. Lett. 130, 050803 (2023).
- [26] H. Jayakumar, A. Predojević, T. Kauten, T. Huber, G. S. Solomon, and G. Weihs, Nature Communications 5, 10.1038/ncomms5251 (2014).
- [27] P. Senellart, G. Solomon, and A. White, Nature Nanotechnology 12, 1026–1039 (2017).
- [28] J. Schneeloch, S. H. Knarr, D. F. Bogorin, M. L. Levangie, C. C. Tison, R. Frank, G. A. Howland, M. L. Fanto, and P. M. Alsing, Journal of Optics 21, 043501 (2019).
- [29] C. Zhang, Y.-F. Huang, B.-H. Liu, C.-F. Li, and G.-C. Guo, Advanced Quantum Technologies 4, 2000132 (2021).
- [30] J.-W. Pan, D. Bouwmeester, H. Weinfurter, and A. Zeilinger, Physical review letters 80, 3891 (1998).
- [31] S. Ramelow, A. Mech, M. Giustina, S. Gröblacher, W. Wieczorek, J. Beyer, A. Lita, B. Calkins, T. Gerrits, S. W. Nam, et al., Optics express 21, 6707 (2013).
- [32] B. Li, S. E. Economou, and E. Barnes, npj Quantum Information 8, 10.1038/s41534-022-00522-6 (2022).
- [33] A. Lamas-Linares, J. C. Howell, and D. Bouwmeester, Nature 412, 887 (2001).
- [34] N. Sangouard, B. Sanguinetti, N. Curtz, N. Gisin, R. Thew, and H. Zbinden, Physical review letters 106, 120403 (2011).
- [35] D. L. P. Vitullo, M. G. Raymer, B. J. Smith, M. Karpiński, L. Mejling, and K. Rottwitt, Phys. Rev. A 98, 023836 (2018).
- [36] H.-S. Zhong, Y. Li, W. Li, L.-C. Peng, Z.-E. Su, Y. Hu, Y.-M. He, X. Ding, W. Zhang, H. Li, L. Zhang, Z. Wang, L. You, X.-L. Wang, X. Jiang, L. Li, Y.-A. Chen, N.-L. Liu, C.-Y. Lu, and J.-W. Pan, Phys. Rev. Lett. 121, 250505 (2018).
- [37] M. Houshmand, M. Houshmand, and J. F. Fitzsimons, Phys. Rev. A 98, 012318 (2018).
- [38] R. Raussendorf, D. E. Browne, and H. J. Briegel, Phys. Rev. A 68, 022312 (2003).
- [39] D. E. Browne, E. Kashefi, M. Mhalla, and S. Perdrix, New Journal of Physics 9, 250–250 (2007).
- [40] S. Bartolucci, P. Birchall, H. Bombín, H. Ca-

- ble, C. Dawson, M. Gimeno-Segovia, E. Johnston, K. Kieling, N. Nickerson, M. Pant, F. Pastawski, T. Rudolph, and C. Sparrow, Nature Communications 14, 10.1038/s41467-023-36493-1 (2023).
- [41] M. C. Löbl, S. Paesani, and A. S. Sørensen, Quantum 8, 1302 (2024).
- [42] M. Pant, D. Towsley, D. Englund, and S. Guha, Nature communications 10, 1070 (2019).
- [43] R. Reichle, D. Leibfried, E. Knill, J. Britton, R. B. Blakestad, J. D. Jost, C. Langer, R. Ozeri, S. Seidelin, and D. J. Wineland, Nature 443, 838 (2006).
- [44] M. D. Eisaman, J. Fan, A. Migdall, and S. V. Polyakov, Review of scientific instruments 82, 071101 (2011).
- [45] A. C. Yao, in 23rd Annual Symposium on Foundations of Computer Science (sfcs 1982) (1982) pp. 160–164.
- [46] O. Goldreich, S. Micali, and A. Wigderson, in Proceedings of the nineteenth annual ACM conference on Theory of computing - STOC '87, STOC '87 (ACM Press, 1987).
- [47] C. Zhao, S. Zhao, M. Zhao, Z. Chen, C.-Z. Gao, H. Li, and Y.-a. Tan, Information Sciences 476, 357–372 (2019).
- [48] D. Beaver, Efficient multiparty protocols using circuit randomization, in *Lecture Notes in Computer Science* (Springer Berlin Heidelberg, 1992) p. 420–432.
- [49] J. B. Nielsen, P. S. Nordholt, C. Orlandi, and S. S. Burra, A new approach to practical active-secure two-party computation, in *Advances in Cryptology - CRYPTO 2012* (Springer Berlin Heidelberg, 2012) p. 681–700.
- [50] I. Damgård, V. Pastro, N. Smart, and S. Zakarias, Multiparty computation from somewhat homomorphic encryption, in *Advances in Cryptology CRYPTO 2012* (Springer Berlin Heidelberg, 2012) p. 643–662.
- [51] A. Choudhury and A. Patra, IEEE Transactions on Information Theory 63, 428–468 (2017).
- [52] Y. Takeuchi, A. Mantri, T. Morimae, A. Mizutani, and J. Fitzsimons, npj Quantum Information 5, 10.1038/s41534-019-0142-2 (2019).
- [53] A. Unnikrishnan and D. Markham, Phys. Rev. A 105, 052420 (2022).
- [54] S. Meesala, S. Wood, D. Lake, P. Chiappina, C. Zhong, A. D. Beyer, M. D. Shaw, L. Jiang, and O. Painter, Nature Physics, 1 (2024).
- [55] S. Mittal, V. V. Orre, A. Restelli, R. Salem, E. A. Gold-schmidt, and M. Hafezi, Physical Review A 96, 043807 (2017).
- [56] K.-H. Luo, H. Herrmann, S. Krapick, B. Brecht, R. Ricken, V. Quiring, H. Suche, W. Sohler, and C. Silberhorn, New Journal of Physics 17, 073039 (2015).
- [57] M. Hein, J. Eisert, and H. J. Briegel, Phys. Rev. A 69, 062311 (2004).
- [58] F. Baccari, R. Augusiak, I. Šupić, J. Tura, and A. Acín, Physical Review Letters 124, 10.1103/physrevlett.124.020402 (2020).
- [59] C. Schön, E. Solano, F. Verstraete, J. I. Cirac, and M. M. Wolf, Physical Review Letters 95, 10.1103/physrevlett.95.110503 (2005).
- [60] S. L. Braunstein and A. Mann, Phys. Rev. A 51, R1727 (1995).
- [61] P. Kok and S. L. Braunstein, Phys. Rev. A 61, 042304 (2000).
- [62] U. Leonhardt and H. Paul, Progress in Quantum Electronics 19, 89 (1995).
- [63] R. Shah, K.-S. Isleif, F. Januschek, A. Lindner, and M. Schott, Journal of Low Temperature Physics 209, 355–362 (2022).

- [64] H. Lee, U. Yurtsever, P. Kok, G. M. Hockney, C. Adami, S. L. Braunstein, and J. P. Dowling, Journal of Modern Optics 51, 1517 (2004).
- [65] R. Rangarajan, M. Goggin, and P. Kwiat, Opt. Express 17, 18920 (2009).
- [66] M. V. Jabir and G. K. Samanta, Scientific Reports 7,
- 12613 (2017).
- [67] F. Steinlechner, S. Ramelow, M. Jofre, M. Gilaberte, T. Jennewein, J. P. Torres, M. W. Mitchell, and V. Pruneri, Opt. Express 21, 11943 (2013).
- [68] M. Medic, J. B. Altepeter, M. A. Hall, M. Patel, and P. Kumar, Opt. Lett. 35, 802 (2010).